

5-2012

An Evaluation of CAPE Tendency in Tornado Outbreaks

Timothy W. Humphrey

University at Albany, State University of New York

Lance F. Bosart

University at Albany, State University of New York

Follow this and additional works at: https://scholarsarchive.library.albany.edu/honorscollege_daes



Part of the [Atmospheric Sciences Commons](#)

Recommended Citation

Humphrey, Timothy W. and Bosart, Lance F., "An Evaluation of CAPE Tendency in Tornado Outbreaks" (2012). *Atmospheric & Environmental Sciences*. 5.

https://scholarsarchive.library.albany.edu/honorscollege_daes/5

This Honors Thesis is brought to you for free and open access by the Honors College at Scholars Archive. It has been accepted for inclusion in Atmospheric & Environmental Sciences by an authorized administrator of Scholars Archive. For more information, please contact scholarsarchive@albany.edu.

An Evaluation of CAPE Tendency in Tornado Outbreaks

Undergraduate Research, ATM 499 Fall 2011-Spring 2012

Date: 15 May 2011

Timothy W. Humphrey and Lance F. Bosart

Department of Atmospheric and Environmental Sciences

University at Albany, State University of New York, Albany, New York

Abstract

Previous studies (e.g., Rasmussen, 2003; Thompson et al., 2003) have examined the impact that instability has on the occurrence of tornadic supercells. However, few studies (e.g., Calas et al., 2000) have examined the impact that the rate of destabilization has on the development of severe convection. Utilizing a CAPE tendency equation derived by Emanuel (1994), this study examines the impact of the rate of atmospheric destabilization on the severity of convection. Comparing six hour analyses of CAPE tendency with observed tornado tracks from the 4-6 May 2007, 5-6 February 2008, and 17 June 2010 tornado outbreaks reveals a potential correlation between CAPE tendency and the occurrence of tornadic supercells. These positive results highlight the need for future research to investigate the impact of CAPE tendency on the severity of convection.

Introduction

During the year of 2011, over 1,700 tornadoes struck portions of the United States. The majority of these tornadoes were produced by a series of outbreaks early in the year. The largest outbreak with a single day record of 122 confirmed tornadoes occurred on 27 April resulting in 316 fatalities and \$4.2 billion in damages (NWS 2011). Additionally, a large number of violent (EF4-EF5) tornadoes struck highly populated areas within the United States. One of the most destructive was the Joplin, Missouri tornado which was the first single tornado to result in over 100 fatalities since 1953 (NWS 2011).

The large number of tornado outbreaks was the result of a combination of persistent conditions favorable for the development of large numbers of tornadic supercells. There are three key ingredients which enhance the likelihood of a tornado outbreak (Craven, 2000; Thompson and Edwards, 2000). The first necessary ingredient is a conditionally unstable atmosphere in which lifted parcels can become buoyant and generate convective thunderstorms. Second, a lifting mechanism (e.g. thermal, surface front, dryline) is needed to form updrafts which transport warm, moist air upwards the level of free convection (LFC). Finally, ambient vertical wind shear is necessary to allow updrafts to rotate and produce supercell thunderstorms (Weisman and Klemp, 1982). Rotation associated with an individual supercell's mesocyclone can then reach the ground and intensify to produce a tornado.

Previous research (e.g., Rasmussen, 2003; Thompson et al., 2003) indicates that moisture and ambient vertical wind shear have an impact on the likelihood of a significant tornado being produced. Enhanced low level moisture lowers the lifted condensation level (LCL) which decreases the distance between the cloud base and the surface. Increased vertical wind shear, particularly in the lowest levels of the troposphere, results in an environment more favorable for low level rotation and potential tornadoes. While increased instability does increase the likelihood of a tornadic supercell, Thompson et. al (2003) found differences in instability were only useful for discriminating between the environments associated with extreme tornadic events and environments associated with no tornadoes. Therefore, Thompson et al. (2003) suggest that instability as represented by the diagnostic parameter of Convective Available Potential Energy (CAPE) is of little use alone in evaluating environments that are more favorable for the development of tornadic supercells.

While the magnitude of CAPE is not useful for determining the environments in which tornadic supercells may form, it is possible that the tendency of CAPE with respect to time may be more useful for discriminating between environments which are more or less favorable for tornadoes to develop. Unfortunately, there are few studies that have utilized CAPE tendency. Calas et. al (2000) analyze CAPE tendency as a diagnostic parameter for forecasting deep convection. However, their analysis focuses on the impact that CAPE tendency may have on convective initiation and not on the severity of convection. Additionally, Calas et. al calculate CAPE tendency through the subtraction of model derived CAPE values between two consecutive hours. Based on the findings of Thompson et. al (2003), the magnitude of CAPE does not sufficiently discriminate between environments where severe deep convection will develop. Therefore, the subtraction of CAPE at two time periods should not be able to discriminate between environments that are more favorable for convective initiation. This corresponds to the finding that CAPE tendency shows no skill in forecasting convective initiation (Calas et. al 2000). However, a physically based calculation of CAPE tendency could potentially show more skill in diagnosing environments where deep convection may be likely to develop.

Emanuel (1994) takes the derivative of CAPE with respect to time to develop a physically based calculation of CAPE tendency. This derivation accounts for processes that act to stabilize or destabilize the atmosphere and are not accounted for in a subtraction of CAPE at two different times. Therefore, Emanuel's CAPE tendency derivation is ideal for examining the potential influence of CAPE tendency on deep convection. The purpose of this paper is to compare CAPE tendency fields with recorded tornado tracks in order to demonstrate the potential use of Emanuel's derivation in forecasting the severity of convection.

CAPE Tendency

a) Derivation of CAPE Tendency

The amount of energy available to drive convective development in a conditionally unstable atmosphere is measured by the diagnostic parameter of CAPE. CAPE is calculated by integrating the buoyancy of an air parcel through the conditionally unstable portion of the atmosphere extending from the level of free convection (LFC) to the equilibrium layer (EL) (Moncrieff and Miller, 1976). The CAPE for a parcel can be expressed as

$$CAPE_i = \int_{p_i}^{p_{LNB_i}} (\alpha_i - \alpha_{env}) dp \quad (1)$$

where p_i represents the pressure of the parcel, p_{LNB_i} the pressure of the EL, α_i the specific volume of the parcel, and α_{env} the specific volume of the environment, respectively. Therefore, the CAPE for a parcel is dependent upon buoyancy differences between the undiluted parcel and the ambient environment. By taking the derivative of equation (Eq.) (1) with respect to time, Emanuel (1994) develops an expression to represent how various large scale processes act to destabilize the atmosphere. This derivation yields an integral as the unsaturated parcel moves through the atmosphere

$$\begin{aligned} \frac{\partial}{\partial \tau} CAPE_i = & \int_{p_i}^{p_{LNB_i}} \left(\frac{\partial \alpha_i}{\partial \tau} - \frac{\partial \alpha_{env}}{\partial \tau} \right) dp + (\alpha_i - \alpha_{env})|_{p_i} \frac{\partial p_i}{\partial \tau} \\ & - (\alpha_i - \alpha_{env})|_{p_{LNB_i}} \frac{\partial p_{LNB_i}}{\partial \tau} \end{aligned} \quad (2)$$

where τ represents time in the reference frame of the parcel within the subcloud layer. The first term on the right hand side of Eq. (2) represents the changing differences in parcel and environmental buoyancy with respect to time. The second term represents the difference in parcel and environmental buoyancy at the initial pressure as the initial pressure changes with time. At the initial pressure of the parcel path, the air parcel has the same specific volume as the environment and results in the second term of Eq. (2) reducing to zero. The third term represents the difference in parcel and environmental buoyancy at the EL as the EL pressure changes with time. However when the parcel reaches the EL, the buoyancy reduces to zero and eliminates the third term. Thus, Eq. (2) simplifies to:

$$\frac{\partial}{\partial \tau} CAPE_i = \int_{p_i}^{p_{LNB_i}} \left(\frac{\partial \alpha_i}{\partial \tau} - \frac{\partial \alpha_{env}}{\partial \tau} \right) dp. \quad (3)$$

However, a parcel does not remain unsaturated as it is lifted through the atmosphere. By utilizing Maxwell's relations, Emanuel relates the change in specific volume at a specific pressure level to fluctuations in entropy, or the influx of energy in the form of heat, and the total water content of the parcel. For the undiluted parcel, the specific can be represented as:

$$\begin{aligned} (\delta \alpha_i)_p &= \delta \left(\frac{\alpha_d}{1 - \gamma_T} \right) = \\ \frac{1}{1 - \gamma_T} \left[(\delta \alpha_d)_p - \frac{\alpha_d}{1 + \gamma_T} (\delta \gamma_T)_p \right] &= \frac{1}{1 - \gamma_T} \left\{ \left(\frac{\partial T}{\partial p} \right)_{s, \gamma_T} \delta s - \right. \\ \left. \left[c_l \ln T \left(\frac{\partial T}{\partial p} \right)_{s, \alpha} + \frac{\alpha_d}{1 + \gamma_T} \right] \delta \gamma_T \right\} \end{aligned} \quad (3.1.1)$$

Terms in Eq. (3.1) multiplied by $\delta \gamma_T$ account for the effects of water on density and heat capacity. Emanuel notes that while not negligible, these processes make a smaller contribution to CAPE than changes in entropy allowing for Eq. (3.1) to be simplified as follows:

$$(\delta \alpha_i)_p \simeq \left(\frac{\partial T}{\partial p} \right)_s \delta s \quad (3.1.2)$$

Differentiating Eq. (3.1.2) with respect to time then yields:

$$\frac{(\delta\alpha_i)_p}{\partial\tau} \simeq \left(\frac{\partial T}{\partial p}\right)_s \frac{\partial s_i}{\partial\tau} \quad (3.1.3)$$

The entropy of the ambient environment can then be represented as:

$$(\delta\alpha_{env})_p \simeq \left(\frac{\partial T}{\partial p}\right)_{s_d} \delta s_d \quad (3.2.1)$$

Taking the time derivative of Eq. (3.2.1) yields:

$$\frac{(\delta\alpha_{env})_p}{\partial\tau} \simeq \left(\frac{\partial T}{\partial p}\right)_{s_d} \frac{\partial s_d}{\partial\tau} \quad (3.2.2)$$

Inserting Eqs. (3.1.3) and (3.2.2) into Eq. (3) produces a CAPE tendency equation of:

$$\frac{\partial}{\partial\tau} CAPE_i = \int_{p_i}^{p_{LNB_i}} \left[\left(\frac{\partial T}{\partial p}\right)_s \frac{\partial s_i}{\partial\tau} - \left(\frac{\partial T}{\partial p}\right)_{s_d} \frac{\partial s_d}{\partial\tau} \right] dp \quad (4)$$

with $\left(\frac{\partial T}{\partial p}\right)_s$ representing the rate of change of temperature with respect to pressure for a constant parcel entropy, $\frac{\partial s_i}{\partial\tau}$ the change in parcel entropy with respect to time, $\left(\frac{\partial T}{\partial p}\right)_{s_d}$ the rate of change of temperature with respect to pressure for a constant environmental entropy, and $\frac{\partial s_d}{\partial\tau}$ the rate of change of atmospheric dry entropy with respect to time.

The first term of Eq. (4) may be directly integrated as follows:

$$\int_{p_i}^{p_{LNB_i}} \left(\frac{\partial T}{\partial p}\right)_s \frac{\partial s_i}{\partial\tau} = (T_i - T_{LNB_i}) \frac{\partial s_i}{\partial\tau} \quad (4.1)$$

with T_i representing the temperature at the beginning of the parcel path and T_{LNB_i} the temperature at the EL. This term represents processes which destabilize the atmosphere by increasing the entropy of the subcloud layer.

While the second term cannot directly be integrated in the entropy form, several substitutions may be made in order to achieve a term that can be integrated. First, the rate of change of temperature with

respect to pressure for a constant environmental entropy is approximated by the dry adiabatic lapse rate

$$\left(\frac{\partial T}{\partial p}\right)_{s_d} \simeq \frac{\alpha}{c_{pd}} \quad (4.2.1)$$

Second, the time rate of change of atmospheric dry entropy is expanded as follows:

$$\frac{\partial s_d}{\partial \tau} = \frac{c_{pd}}{\theta} \frac{\partial \theta}{\partial \tau} = \frac{\dot{Q}}{T} - \frac{c_{pd}}{\theta} \left(V_r \cdot \nabla \theta + \omega \frac{\partial \theta}{\partial p} \right) \quad (4.2.2)$$

Inserting Eqs. (4.2.1) and (4.2.2) into Eq. (4) and making the hydrostatic approximation yields Eq. (5):

$$\frac{\partial}{\partial \tau} CAPE_i \simeq \underbrace{\left(T_i - T_{LNB_i} \right) \frac{\partial s_i}{\partial \tau}}_{\text{Term A}} - \int_{z_i}^{z_{LNB_i}} \left(\underbrace{\frac{g \dot{Q}}{c_{pd} T}}_{\text{Term B}} - \underbrace{\frac{g}{\theta} V_r \cdot \nabla \theta}_{\text{Term C}} - \underbrace{N^2 \omega}_{\text{Term D}} \right) dz$$

where τ represents time, T_i the temperature at the beginning of the parcel path, T_{LNB_i} the temperature at the EL, $\frac{\partial s_i}{\partial \tau}$ the change of parcel entropy in the subcloud layer, z_i the height of the LCL, z_{LNB_i} the height of the EL, g gravity, c_{pd} the specific heat capacity of dry air, θ potential temperature, V_r the horizontal velocity relative to the coordinate system translating with the surface parcel, and N^2 the Brunt–Väisälä frequency, and ω the vertical motion, respectively. This final form of the CAPE tendency equation states that the atmosphere is destabilized by processes that increase the entropy of the subcloud layer and processes which decrease the temperature profile of the free atmosphere above the LCL.

Term A of Eq. (5) represents processes which act to increase the entropy within the portion of the atmosphere below the LCL, henceforth referred to as the subcloud layer. In the subcloud layer, entropy measures the transfer of energy into the parcel in the form of heat. With the subcloud layer being unsaturated, the time rate of change of parcel entropy can be represented by multiplying the specific heat capacity of dry air by the total time rate of change of the parcel temperature. However, this simplification results in units of $J K kg^{-1} s^{-1}$. Therefore, in order to achieve the correct CAPE tendency units of $J kg^{-1} s^{-1}$, the difference in temperature of the parcel and the temperature at the equilibrium layer must be normalized. This normalization is accomplished by dividing $(T_i - T_{LNB_i})$ by T_i and

resulting in the total time rate of change of temperature to be multiplied by a fraction of the specific heat capacity of dry air. Thus, the final form of the subcloud entropy term is represented by

$$\left(1 - \frac{T_{LNB_i}}{T_i}\right) c_{pd} \frac{DT}{D\tau}$$

Therefore, Term A shows an increase in the temperature of the subcloud layer will destabilize the atmosphere. This can be accomplished through diurnal heating, horizontal temperature advection, adiabatic warming of descending air, or a combination of these three large scale processes acting to alter the LCL height and resulting depth of the subcloud layer.

In addition to heating of the subcloud layer, processes which cool the free atmosphere above the LCL act to destabilize the atmosphere. These processes are represented by the final three terms in Eq. (5) which are integrated from the LCL to the EL. Term B represents the radiative cooling of the free atmosphere through the emission of longwave radiation. The cooling at a given height is represented by

$$\frac{g\dot{Q}}{c_{pd}T}$$

with T representing the environmental temperature and \dot{Q} representing the radiative cooling rate of the free atmosphere, which is approximately 2 K day^{-1} . As the height from the surface increases, the temperature gradient between model grid points decreases. Therefore, when summed from the LCL to the EL, Term B displays little to no horizontal variation over the synoptic scale.

Horizontal cold air advection above the LCL can also act to decrease the temperature profile and destabilize the atmosphere. This process is represented by Term C:

$$\int_{z_i}^{z_{LNB_i}} -\frac{g}{\theta} V_r \cdot \nabla \theta dz$$

In Term C, V_r is the horizontal velocity relative to a coordinate system translating with the surface parcel. Therefore, when calculating CAPE tendency from gridded datasets, the surface parcel must be tagged in order to calculate the relative velocity at each level. In this study, surface parcels are tagged by calculating the twelve hour average motion of the surface cyclone which provides the forcing for convective development. The center of the surface cyclone is recorded six hours prior to and six hours after the analysis period. The distance and bearing of the cyclone center is then input into a Java calculator (Appendix I) to determine the meridional and zonal components of the cyclone motion. The components are then subtracted from the vector wind at each vertical level in the dataset to generate a horizontal velocity relative to the surface parcel. The dot product of the relative velocity and the horizontal potential temperature gradient is calculated and summed from the LCL to the EL. In regions

where there is net cold air advection above the LCL the atmosphere will destabilize and make a positive contribution to CAPE tendency.

In addition to horizontal advection, vertical motion (advection) acts to adjust the environmental lapse rate within a layer of the atmosphere. The contribution of vertical motion to CAPE tendency is represented by Term D

$$\int_{z_i}^{z_{LNB_i}} -N^2 \omega dz$$

where ω synoptic scale vertical motion and N^2 represents the Brunt–Väisälä, or buoyancy frequency, of a layer of the atmosphere. The buoyancy frequency can be expanded

$$N^2 = \frac{g}{\theta_0} \frac{\partial \bar{\theta}}{\partial z}$$

to show that the buoyancy of a layer of the free atmosphere is dependent upon the potential temperature of the bottom of the layer and the environmental lapse rate.

b) Scale Analysis

For midlatitude deep convection, all four processes have an impact on CAPE tendency. Therefore, it is important to estimate the order of magnitude of each term in order to gauge their relative importance in destabilizing the atmosphere. Squall lines represent the most widespread convection and can range in horizontal length from 10 km to over 100 km. As a result, all terms in the CAPE tendency equation will be approximated according to the mesoscale (Holton, 2004). Additionally, all terms will be scaled to $(6 \text{ h})^{-1}$ to facilitate comparison with the computed CAPE tendency.

When scaling Term A, T_i and T_{LNB_i} are both on the order of 10^2 K . However, T_{LNB_i} is less than T_i in the atmosphere resulting in the constant before c_{pd} being on the order of 10^{-2} . c_{pd} is scaled by $10^3 \text{ J kg}^{-1} \text{ K}^{-1}$. In a mesoscale environment where strong diurnal heating is occurring, the local temperature can increase by 10 K over six hours. Meanwhile, winds within the subcloud layer can be on the order of 10^1 ms^{-1} and act on temperature gradients which can be scaled by $10^1 \text{ K} (10^5 \text{ m})^{-1}$. Emanuel (1994) notes that mesoscale updrafts can achieve vertical velocities of one to two ms^{-1} . Finally, the vertical temperature gradient in the troposphere is on the order of 10^1 K . Combining these scaling terms as follows:

$$\left(\mathbf{1} - \frac{T_{LNB_i}}{T_i} \right) c_{pd} \left(\frac{\partial T}{\partial \tau} + u \frac{\partial T}{\partial x} + v \frac{\partial T}{\partial y} + w \frac{\partial T}{\partial z} \right)$$

$$\begin{aligned}
& (\mathbf{10^{-2}})(\mathbf{10^3 Jkg^{-1}K^{-1}}) \left[\left(\frac{\mathbf{10^1 K}}{(\mathbf{6 h})^{-1}} \right) \right. \\
& \quad + \mathbf{10^1 ms^{-1}} \left(\frac{\mathbf{10^1 K}}{\mathbf{10^5 m}} \right) \left(\frac{\mathbf{10^4 s}}{\mathbf{6 h}} \right) \\
& \quad + \mathbf{10^1 ms^{-1}} \left(\frac{\mathbf{10^1 K}}{\mathbf{10^5 m}} \right) \left(\frac{\mathbf{10^4 s}}{\mathbf{6 h}} \right) \\
& \quad \left. + \mathbf{10^0 ms^{-1}} \left(\frac{\mathbf{10^1 K}}{\mathbf{10^4 m}} \right) \left(\frac{\mathbf{10^4 s}}{\mathbf{6 h}} \right) \right] \\
& = (\mathbf{10^{-2}})(\mathbf{10^3 Jkg^{-1}K^{-1}}) \left[\left(\frac{\mathbf{10^1 K}}{(\mathbf{6 h})^{-1}} \right) \right. \\
& \quad \left. + \left(\frac{\mathbf{10^1 K}}{(\mathbf{6 h})^{-1}} \right) + \left(\frac{\mathbf{10^1 K}}{(\mathbf{6 h})^{-1}} \right) + \left(\frac{\mathbf{10^1 K}}{(\mathbf{6 h})^{-1}} \right) \right] \\
& = \mathbf{10^2 Jkg^{-1}(6 h)^{-1}}
\end{aligned}$$

reveals that Term A contributes roughly $100 \text{ J kg}^{-1} (\text{6 h})^{-1}$.

In Term B, g scales to 10^1 ms^{-2} and Q to 2 K day^{-1} . This results in Term B scaling to $10 \text{ J kg}^{-1} (\text{6 h})^{-1}$.

Plugging in the previously stated mesoscale approximations into Terms C and D reveals they are also on the order of $10 \text{ J kg}^{-1} (\text{6 h})^{-1}$. Therefore, for deep midlatitude convection processes that increase subcloud entropy are dominant in destabilizing the atmosphere. This corresponds to previous sensitivity studies (e.g. Crook, 1996) which indicate that low level moisture and temperature changes have the largest impact on the magnitude of CAPE. While radiative cooling, horizontal and vertical temperature advection are an order of magnitude smaller than the subcloud entropy term, they can contribute to local maxima in CAPE tendency which can distinguish environments over small distances.

Data and Methodology

This study utilizes the datasets from the National Centers for Environmental Prediction's (NCEP) Climate Forecast System Reanalysis (CFSR) Version I (Saha et al. 2010). CFSR is a coupled atmosphere-ocean-land surface-sea ice model which produces global gridded estimates of the state of each field over a domain extending from January 1979 through March 2011. The data has a horizontal resolution of 0.5°

latitude X 0.5° longitude which results in an approximate grid spacing of 38 km. This horizontal resolution is only slightly coarser than regional reanalysis datasets such as the NCEP North American Regional Reanalysis which has a horizontal resolution of approximately 32 km (Mesinger et al., 2006). Gridded atmospheric data consists of 37 pressure levels with a vertical resolution of 25 hPa from the surface to 750 hPa and 50 hPa from 750 hPa to 100 hPa. The temporal resolution of the CFSR dataset is six hours with analyses available at 0000, 0600, 1200, and 1800 UTC (Saha et al. 2010). The high horizontal, vertical, and temporal resolution of the CFSR data combined with the global grid coverage and coupled climate system physics supplements this study's goal of examining how accurately Emanuel's CAPE tendency derivation represents the severity of convection.

Utilizing the NCEP Storm Prediction Center's (SPC) Severe Weather Events Archive [available online at: <http://www.spc.noaa.gov/exper/archive/events/>], tornado outbreaks are identified by selecting dates where over 20 tornadoes were reported in the continental United States. CFSR data is then downloaded for six hours prior to the closest analysis period of the first reported tornado through six hours after the analysis closest to the last reported tornado. CAPE tendency is then calculated in the General Meteorological Package (GEMPAK; desJardins and Petersen, 1985) utilizing a series of shell scripts (provided in Appendix II) for each six hour analysis throughout the duration of the outbreak. However, the vertical frame of reference in the CFSR dataset is pressure while the CAPE tendency derivation utilizes a vertical reference frame of height. Therefore, the CAPE tendency derivation must be converted to a pressure coordinate form. Substituting in for dz utilizing relationships from the Ideal Gas Law and hydrostatic balance yields a pressure coordinate form of Eq. (5) as follows:

$$\frac{\partial}{\partial \tau} CAPE_i \simeq (T_i - T_{LNB_i}) \frac{\partial s_i}{\partial \tau} - \int_{p_i}^{p_{LNB_i}} \left(\frac{g\dot{Q}}{c_{pd}T} - \frac{g}{\theta} V_r \cdot \nabla \theta - N^2 \omega \right) \frac{-R_d T}{pg} dp$$

where R_d represents the gas constant of dry air. This form (Eq. 6) of the CAPE tendency is then calculated and mapped in GEMPAK. To examine the effectiveness of CAPE tendency in representing the severity of convection, tornado tracks were plotted in SPC's Online SeverePlot 3.0 [available at: <http://www.spc.noaa.gov/climo/online/sp3/plot.php>] and compared with mapped CAPE tendency. Should CAPE tendency have an impact on the severity of convection, observed tornado tracks are expected to be collocated with maxima in CAPE tendency.

Sources of Error

While Eq. (6) represents the physical processes that act to destabilize the atmosphere with reasonable accuracy, the conversion of the equation to a computer language introduce errors in the calculation of

CAPE tendency. First, microphysical assumptions made in the derivation and microphysical parameterization schemes within the CFSR introduce errors. Second, errors arise when the virtual temperature correction is not included in the derivation of CAPE tendency. However, Doswell and Rasmussen (1994) note that these errors are not significant in situations where large CAPE (on the order of 3000 J kg^{-1}) is present. Since the cases analyzed involve widespread tornado outbreaks, ample CAPE should be present for the development of supercell thunderstorms over a large area. Third, vertical layers are rounded to the nearest 50 hPa due to the resolution of the CFSR. Fourth, Terms B, C, and D cannot be calculated for different layers at individual gridpoints. Therefore, calculating the terms on the right hand side of Eq. (6) over fixed 50 hPa layers require that the LCL and EL are constant across the entire globe. This results in positive values of CAPE tendency appearing where no CAPE is present. However, we can mitigate this unphysical situation by utilizing a Boolean mask which removes CAPE tendency that are sufficiently far from areas where CAPE is not present. Finally, instantaneous values of advection, vertical motion, and other physical processes are extrapolated to six hour time frames. We attempt to mitigate errors that arise from extrapolation by defining the per six hour period as three hours prior to and three hours after the time of analysis.

In addition to errors which arise from the derivation and programming of CAPE tendency, variations in the magnitude of CAPE tendency arise based on the selection of initial parcel pressure (Bunkers et al., 2002; Rochette et al., 1999). Surface based (SB) CAPE is measures the parcel path with respect to the surface temperature and moisture content. When representing SB convection, SBCAPE is the ideal choice for diagnosing atmospheric instability. However, during the overnight period SBCAPE frequently reduces to zero as an inversion develops above the surface (Bunkers et al., 2002). Calculating CAPE with respect to the most unstable (MU) parcel within the lowest 300 hPa of the atmosphere results in MUCAPE which can more accurately represent the energy available for nocturnal convection which is elevated above the surface (Rochette et al., 1999). CAPE can also be calculated with respect to a theoretical parcel that would originate from a well-mixed layer (ML) (Bunkers et al., 2002). However, the selection of the size of the ML used to calculate MLCAPE is subjective (e.g. Bluestein and Jain, 1985; Johns et al., 1993; Rasmussen and Blanchard, 1998). Due to the potential inaccuracies that arise from SBCAPE and MLCAPE, Doswell and Rasmussen (1994) and Rochette et al. (1999) recommend that MUCAPE be used to assess atmospheric instability. Despite the accuracy of MUCAPE, this study utilizes SB parcels in order to calculate CAPE tendency in order to facilitate comparison between multiple cases.

Case Studies

Three case studies are presented to illustrate how CAPE tendency performs in representing tornado outbreaks associated with different types of synoptic forcing. The three types of tornado outbreaks which will be examined include those associated with: a developing cyclone, a mature cyclone, and weak synoptic forcing. Each case study will present a synoptic overview of the outbreak and a comparison of computed CAPE tendency with observations of tornadic supercells on satellite and radar along with recorded tornado tracks.

a) Developing Cyclone

On 4-6 May 2007, a developing surface cyclone in the western Great Plains generated an environment favorable for supercells and tornadoes. By 1200 UTC 7 May 2007, 128 tornadoes had touched down resulting in \$268 million in damages and 14 fatalities (National Climatic Data Center [NCDC]).

At 1200 UTC 4 May 2007, a 300 hPa trough is centered over the west coast of the United States with the poleward exit region of the 40 ms^{-1} jet streak extending over Colorado (Fig. 1). A maxima in 500 hPa cyclonic vorticity advection collocated beneath a 300 hPa divergence maxima over Colorado results in a region of ascent favorable for the development of a cyclone lee of the Rocky Mountains. The developing cyclonic circulation results in southerly winds extending from the surface to 850 hPa advecting a maritime tropical airmass from the Gulf of Mexico into the Great Plains. Surface temperatures exceeding $25 \text{ }^\circ\text{C}$ combined with $20 \text{ }^\circ\text{C}$ dewpoints destabilize the boundary layer over Texas, Oklahoma, Kansas, and Nebraska while westerly flow at 300 and 500 hPa advects colder air over the Great Plains (Fig. 2).

As diurnal heating increases through 1800 UTC, the boundary layer over the Great Plains continues to destabilize. The 1800 UTC 4 May CAPE tendency analysis displays three regions with CAPE tendency exceeding $400 \text{ J kg}^{-1} (6 \text{ h})^{-1}$ (Fig. 3). One maximum exists along the surface warm front extending from portions of the Mississippi River Valley to Nebraska. Ongoing convection located near the $400 \text{ J kg}^{-1} (6 \text{ h})^{-1}$ maximum in Nebraska produces several reports of large hail but no tornadoes (Fig. 4). Meanwhile, in regions of Missouri, Kansas, and Oklahoma, where skies are clear, CAPE tendency exceeds $800 \text{ J kg}^{-1} (6 \text{ h})^{-1}$ and is aiding in the development of scattered cumulus (CU) in the satellite imagery (Fig. 3). In western Colorado, differential heating of the elevated terrain coupled with strong cold air advection near the upper level low is contributing to a CAPE tendency maximum exceeding $3200 \text{ J kg}^{-1} (6 \text{ h})^{-1}$. A third maximum in CAPE tendency extends along and ahead of the surface dryline from western Kansas through the Oklahoma panhandle into central Texas. 1825 UTC satellite imagery indicates a CU field west of the Oklahoma panhandle. Southwesterly flow extending from 800 hPa to the EL at 200 hPa will advect this CU field into areas where the atmosphere is destabilizing in excess of $800 \text{ J kg}^{-1} (6 \text{ h})^{-1}$.

By 0000 UTC 5 May, the magnitude of the three maxima in CAPE tendency decreases due to the reduction of diurnal heating (Fig. 5). The CU field over the Oklahoma panhandle consolidates as two supercell thunderstorms develop on satellite and radar. The anvil shadows from these supercells could be contributing to the relative minimum in CAPE tendency by cooling the boundary layer over central Oklahoma and Kansas (Markowski, 2005). Meanwhile, 0015 UTC visible satellite imagery also indicates a field of cumulonimbus (CB) over eastern Colorado where CAPE tendency exceeds $400 \text{ J kg}^{-1} (6 \text{ h})^{-1}$. These CB produce hail in excess of 5.1 cm and one tornado within the maximum of CAPE tendency (Fig. 6). Additional tornadoes reported in central Kansas, North Dakota, and Oklahoma, are also collocated with regional maxima in CAPE tendency.

The 0600 CAPE tendency analysis reveals that CAPE tendency associated with the dryline and warm front evolve in very different fashions during the overnight period (Fig. 7). The 0600 UTC CAPE tendency associated with the warm front remains above $200 \text{ J kg}^{-1} (6 \text{ h})^{-1}$. However, along the dryline the CAPE tendency signal disappears entirely. As the dryline retreats to the west after 0000 UTC 5 May, increasing low level moisture acts to increase the magnitude of CAPE to over 5000 J kg^{-1} (Fig. 8). Meanwhile, the low level jet (LLJ) over Kansas strengthens and results in 0-1km helicity increasing from 59 to $414 \text{ m}^2\text{s}^{-2}$ by 0500 UTC 5 May (Lemon and Umisheid, 2008). The extreme combination of high instability and strong low level shear support the development of a rare EF-5 tornado which destroys 90% of Greensburg, Kansas (Lemon and Umisheid, 2008; McCarthy et al., 2007). This discrepancy in observed and calculated CAPE tendency is disconcerting. One possible explanation is that the 0600 UTC

5 May CFSR analysis is too far removed from the time frame in which the dryline retreats to accurately represent the destabilization associated with increasing low level moisture. Another explanation for this discrepancy is that SBCAPE may not provide the most accurate representation of instability due to the development of low level inversions during the overnight period (Bunkers et al., 2002). Future evaluations of CAPE tendency utilizing analyses with high temporal resolution from the Rapid Update Cycle or a similar model could determine which of these hypotheses most accurately explains the discrepancy.

At 1200 UTC 5 May, the surface warm front extends from Arkansas through Missouri to the Nebraska-South Dakota border (Fig. 9). The 1200 UTC maxima in CAPE tendency are located just to the south and east of the front where the greatest temperature and moisture advection is occurring (Fig. 10). In eastern Nebraska, precipitation associated with ongoing convection decreases the surface temperature and the associated decrease in subcloud entropy results in a minimum in CAPE tendency over the area. As diurnal heating increases through 1800 UTC 5 May, several maxima in CAPE tendency develop. The first maximum extends along the dryline from central Texas to the Oklahoma panhandle with CAPE tendency exceeding $800 \text{ J kg}^{-1} (6 \text{ h})^{-1}$ in several regions (Fig. 11). The second maximum is located over Colorado and western Nebraska where cold air advection associated with the cold core of the upper level low is maximized. A third, weaker maximum in CAPE tendency extends along the warm front from eastern Nebraska to eastern South Dakota. Anvil shading from ongoing convection in the 1825 UTC satellite imagery is a possible cause of the two CAPE tendency minima in Nebraska and South Dakota. Meanwhile convection developing along the dryline is steered toward the northeast by the upper level flow and moves over the axis of CAPE tendency. However, from 1500 UTC to 2100 UTC 5 May no tornadoes are reported in Oklahoma while several are observed in Nebraska (Fig. 12). Despite the lower CAPE tendency present, in portions of Nebraska SBCAPE exceeds 2000 J kg^{-1} and 0-1km helicity ranges from 250 to $400 \text{ m}^2\text{s}^{-2}$. This enhanced helicity and high instability results in an environment favorable for tornadoes (Thompson et al. 2003) and likely compensates for the weaker rate of destabilization.

Between 1800 UTC 5 May and 0000 UTC 6 May, another line of supercells develops from central Kansas to the Oklahoma panhandle (Fig. 13). The 0000 UTC CAPE tendency analysis indicates the atmosphere across this region is destabilizing at a rate of over $200 \text{ J kg}^{-1} (6 \text{ h})^{-1}$. Meanwhile, two regions where CAPE tendency exceeds $1600 \text{ J kg}^{-1} (6 \text{ h})^{-1}$ are present in northeastern Missouri and western South Dakota. With the atmosphere continuing to destabilize and 0-1 km helicity exceeding $150 \text{ m}^2\text{s}^{-2}$, the atmosphere should be favorable for severe deep convection. This is confirmed in the 0015 UTC satellite imagery where overshooting tops within the CB field indicate where updrafts have extended into the lower stratosphere. These strong supercell thunderstorms move to the northeast following the upper tropospheric flow and produce 72 reported tornadoes between 2100 UTC 5 May and 0300 6 May (NCDC). The observed tornado tracks in central Kansas and western Oklahoma are collocated with maxima in the 0000 UTC 6 May CAPE tendency analysis despite the contamination that could be occurring due to anvil shading (Fig. 14). Additional tornado families occur in eastern South Dakota and southwestern Iowa, where the atmospheric CAPE tendency is over $400 \text{ J kg}^{-1} (6 \text{ h})^{-1}$ and 0-1 km helicity exceeds $300 \text{ m}^2\text{s}^{-2}$.

After 0000 UTC 6 May, the persistent release of latent heat by ongoing convection results in the height pattern at 300 and 500 hPa over the Great Plains taking on a more meridional orientation (Fig. 15). The backing of the upper level winds results in a unidirectional wind shear vector which favors multicell clusters and bowing segments (Lee et al., 1992). The ongoing supercells began to merge and by 0600

UTC 6 May formed a squall line extending from Iowa to Oklahoma (Fig. 16). From 0300 UTC to 0900 UTC, nine tornadoes are reported in portions of Kansas, Iowa, Texas, and Oklahoma (NCDC, Fig. 17). However, the 0600 UTC analysis of CAPE tendency does not indicate destabilization (Fig. 16). Once again, the validity of calculating SBCAPE tendency from the 0600 UTC analysis comes into question and remains an area of future research. Despite these discrepancies in the 0600 UTC 5 May and 6 May analyses, the comparison of analyzed CAPE tendency and observed tornado tracks during the 4-6 May tornado outbreak reveal a potential correlation between the rate of destabilization and the occurrence of tornadoes.

b) Mature Cyclone

The “Super Tuesday” tornado outbreak is associated with a cyclone that developed lee of the Rocky Mountains and quickly moved through the Mississippi and Tennessee River Valleys from 5-6 February 2008. The unseasonably warm and moist airmass combined with strong deep and low-level shear produces an environment favorable for supercell thunderstorms to develop. These supercells produce 87 tornadoes which result in over \$530 million in damages (NWS, 2009). Additionally, the 25 ms^{-1} forward motion of the thunderstorms make it difficult for people in the path of the tornadoes to take cover, resulting in 57 fatalities (NWS, 2009).

On 3 February 2008, a developing surface cyclone over the Rocky Mountains and a high pressure centered off the east coast of the United States produce surface southerly flow across the Southern Plains and Southeast. Over the next two days, a maritime tropical airmass characterized by surface temperatures above $20 \text{ }^\circ\text{C}$ and dewpoints near $18 \text{ }^\circ\text{C}$ is advected into the region producing a conditionally unstable atmosphere (Fig. 18). As the 300 hPa trough moves over the region through 1200 UTC 5 February, veering winds with height produce vertical wind shear favorable for the development of rotating updrafts and supercell thunderstorms. Divergence associated with the equatorward entrance region of the 50 ms^{-1} jet also deepens the surface cyclone and associated cyclonic circulation (Fig. 19). This develops a strong cold front from Oklahoma through Texas with surface temperatures below 10°C behind the front. As the surface cyclone progresses to the northeast, the cold front acts as a lifting mechanism which triggers the development of convection.

The 1800 UTC analysis of CAPE tendency reveals a broad area of destabilization within the warm sector of the cyclone (Fig. 20). The atmosphere over Mississippi, Louisiana, and southern Arkansas, is destabilizing the most rapidly with CAPE tendency exceeding $400 \text{ J kg}^{-1} (6 \text{ h})^{-1}$. Additionally, the LLJ at 800 hPa increases to over 25 ms^{-1} enhancing the environmental bulk shear and helicity. Despite the favorable environment for supercell thunderstorms, a temperature inversion at 700 hPa indicated by the Little Rock, Arkansas 1800 UTC sounding is inhibiting the development of SB convection (Fig. 21). The majority of convection is occurring in proximity to the surface cold front and produces isolated reports of severe hail and wind damage (Fig. 22).

By 0000 UTC 6 February, the inversion erodes allowing for convection to release the 1495 J kg^{-1} of SBCAPE. This results in several supercell thunderstorms developing ahead of the surface cold front in portions of Arkansas and Mississippi. As these supercells move to the northeast, they enter an

environment that is continuing to destabilize at the rate of $200 \text{ J kg}^{-1} (6 \text{ h})^{-1}$ (Fig. 23). Meanwhile, the LLJ strengthens closer to the surface and increases the 0-1 km helicity to $400 \text{ m}^2 \text{ s}^{-2}$. Mead and Thompson (2011) find that environments that continue to destabilize after 0000 UTC are more favorable for the development of significant nocturnal tornadoes. The environmental helicity values at 0000 UTC are also above the median associated with significant tornadoes in Thompson et al. (2003). Therefore, the atmosphere over the Tennessee River Valley at 0000 UTC 6 February is conducive for the development of significant tornadoes. Between 2100 UTC 5 February and 0300 UTC 6 February, 48 tornadoes are reported, including several long track tornadoes rated stronger than EF-3 (NWS, 2009; Fig. 24).

With the loss of diurnal heating after 0000 UTC, CAPE tendency within the warm sector rapidly decreases from 0000 UTC to 0600 UTC 6 February (Fig. 25). Meanwhile, the 0000 UTC sounding from Nashville, Tennessee (BNA) indicates that convection moving into the region will likely become elevated (Fig. 26). Therefore, the lack of large regions of destabilization in the 0600 UTC CAPE tendency analysis is not surprising. From 0300 UTC to 0900 UTC, several tornadoes are reported along the periphery of the $200 \text{ J kg}^{-1} (6 \text{ h})^{-1}$ maximum in eastern Tennessee. Additional tornadoes are reported in Mississippi and Alabama, where enhanced helicity compensates for the lower magnitudes of CAPE (Fig. 27).

c) Weak Synoptic Forcing

At 1200 UTC 17 June 2010, an upper level trough and associated 1000 hPa surface cyclone is located over the Rocky Mountains (Fig. 28). Southeasterly flow ahead of the cyclone is advecting warm moist air from the Gulf of Mexico into the Northern Plains. However, no distinct surface warm front is present in North Dakota and Minnesota to provide forcing for ascent (Fig. 29). Several shortwave impulses are forecast to be advected ahead of the upper level trough and could provide forcing for ascent.

As diurnal heating increases through 1800 UTC, a $800 \text{ J kg}^{-1} (6 \text{ h})^{-1}$ maximum in CAPE tendency develops from North Dakota through Nebraska and Kansas where skies have cleared (Fig. 30). A relative minimum exists over central North Dakota due to cloud cover associated with CB that develops. A second maximum in CAPE tendency extends from Wisconsin through Minnesota into North Dakota. A field of CU exists along a surface boundary to the south and east of this secondary maximum and is propagating to the north and east. As this boundary moves into the region of greater than $800 \text{ J kg}^{-1} (6 \text{ h})^{-1}$ CAPE tendency in Minnesota, convection rapidly develops between 2000 UTC and 2100 UTC (Fig. 30). Between 1500 UTC and 2100 UTC, ten tornadoes are reported in North Dakota and Minnesota. The tornadoes in Minnesota are collocated with the secondary maximum in the 1800 UTC CAPE tendency analysis (Fig. 31). While the observed tornado tracks in North Dakota are collocated with weak or no CAPE tendency, enhanced low level helicity in the region possible compensated for the weaker rate of destabilization.

After 0000 UTC 18 June, CAPE tendency decreases due to a decrease in diurnal heating (Fig. 32). However, a region of CAPE tendency is collocated with clearing skies over the North Dakota-Minnesota border. Ongoing convection extending from Minnesota through Iowa is moving into a region of CAPE tendency exceeding $200 \text{ J kg}^{-1} (6 \text{ h})^{-1}$. Behind the CB where skies are clearing, another region of CAPE tendency is analyzed. When comparing the observed tornado tracks with the 0000 UTC CAPE tendency

analysis, tornadoes in southern Minnesota and northern Iowa are collocated with maxima in CAPE tendency (Fig. 33). Meanwhile, there is no correlation between CAPE tendency and the observed tornadoes in northern Minnesota and North Dakota. However, 34 of these tornadoes were reported between 2100 and 2230 UTC (NCDC). Therefore, the 0000 UTC CAPE tendency analysis may not accurately represent the environment in which these tornadoes occurred.

After 0000 UTC, CAPE tendency rapidly decreases across the region. The 0600 UTC analysis the only maxima in CAPE tendency present in the Mississippi River Valley (Fig. 34). The decreasing instability results in the convection weakening through the overnight period and only two tornadoes reported just after 0300 UTC. These two tornadoes brought the total confirmed tornadoes to 74 (NCDC). Through the duration of the event, the performance of CAPE tendency varies with respect to representing the severity of convection. While the 1800 UTC analysis has maxima collocated with observed tornado tracks, the 0000 UTC analysis shows large disconnects in the location of CAPE tendency and the observed tornado tracks. However, as previously noted, the temporal resolution of the CFSR dataset may not be sufficient to represent the convection occurring between 2000 UTC and 2300 UTC 17 June.

Conclusions

Previous studies (e.g. Rasmussen, 1998, 2003; Thompson et al., 2003) examining environments favorable for the development of tornadic supercells have focused on the magnitude of CAPE as a possible discriminating parameter. Little research has been conducted on how the rate of atmospheric destabilization may impact the severity of convection. Only Calas et al. (2000) examines CAPE tendency as a parameter for forecasting convective initiation. However, Calas et al. (2000) calculates CAPE tendency by subtracting CAPE between two subsequent hours. A physically based equation for CAPE tendency derived by Emanuel (1994) is utilized to examine the impact atmospheric destabilization has on the severity of convection.

CAPE tendency is evaluated calculating from the CFSR dataset for three tornado outbreaks with different synoptic forcing and comparing the analyses to observed tornado tracks. For the three tornado outbreaks, tornado tracks are frequently collocated with maxima in CAPE tendency. This indicates a potential correlation between the rate of atmospheric destabilization and the severity of developing or ongoing convection in the area. However, tornado tracks often did not correspond to maxima in the 0600 UTC CAPE tendency analyses. These discrepancies could possibly be due to the temporal resolution of the CFSR dataset or convection becoming elevated during the overnight hours. Despite these persistent discrepancies, the positive results from the majority of the analyses indicate that Emanuel's CAPE tendency derivation accurately represents atmospheric destabilization. Therefore, future research should be conducted to further examine the potential correlation between atmospheric destabilization and the severity of midlatitude convection.

Acknowledgments

I would like to acknowledge the following people for their contributions to this research project: Kristen Corbosiero, Kyle Griffin, Andrea Lang, Ross Lazear, Ryan Torn, and Kevin Tyle. I would also like to thank

Lance Bosart and Kerry Emanuel for presenting me this opportunity and for their guidance throughout the research process.

References

- Bluestein, H. B., and M. H. Jain, 1985: Formation of mesoscale lines of precipitation: Severe squall lines in Oklahoma during the spring. *J. Atmos. Sci.*, **42**, 1711-1732.
- Bunkers, M. J., B. A. Klimowski, and J. W. Zeitler, 2002: The importance of parcel choice and the measure of vertical wind shear in evaluating the convective environment. Preprints, *21st Conf. on Severe Local Storms*, San Antonio, TX, Amer. Meteor. Soc., 379-382.
- Calas, C., V. Ducrocq, and S. Se'ne'si, 2000: Mesoscale analyses and diagnostic parameters for deep convection nowcasting. *Meteor. Appl.*, **7**, 143-161.
- Craven, J. P., 2000: A preliminary look at deep layer shear and middle level lapse rates during major tornado outbreaks. Preprints, *20th Conf. on Severe Local Storms*, Orlando, Amer. Meteor. Soc., 547-550.
- Crook, N. A., 1996: Sensitivity of Moist Convection Forced by Boundary Layer Processes to Low-Level Thermodynamic Fields. *Mon. Wea. Rev.*, **124**, 1767-1785.
- desJardins, M. L., and R. A. Petersen, 1985: GEMPAK A meteorological system for research and education. Preprints, *First International Conf. on Interactive Information and Processing Systems for Meteorology, Oceanography, and Hydrology*, Los Angeles, Amer. Meteor. Soc., 313-319.
- Doswell, C. A., III, III, and E. N. Rasmussen, 1994: The effect of neglecting the virtual temperature correction on CAPE calculations. *Wea. Forecasting*, **9**, 625-629.
- Emanuel, K. A., 1994: *Atmospheric Convection*, 592 pp.
- Holton, J. R., 2004: *An Introduction to Dynamic Meteorology*. 4th ed. Academic Press, 511 pp.
- Johns, R. H., J. M. Davies, and P. W. Leftwich, 1993: Some wind and instability parameters associated with strong and violent tornadoes. 2. Variations in the combinations of wind and instability parameters. *The Tornado: Its Structure, Dynamics, Prediction, and Hazards*, Geophys. Monogr., No. 79, Amer. Geophys. Union, 583-590.
- Lee, W.-C., R. E. Carbone, and R. M. Wakimoto, 1992: The evolution and structure of a "bow-echo-microburst" event. Part I: The bow echo. *Mon. Wea. Rev.*, **120**, 2188-2210.
- Lemon, L. R., and M. Umscheid, 2008: The Greensburg, Kansas tornadic storm: A storm of extremes. Preprints, *24th Conf. on Severe Local Storms*, Savannah, GA, Amer. Meteor. Soc., 2.4
- Markowski, Paul M., Jerry Y. Harrington, 2005: A Simulation of a Supercell Thunderstorm with Emulated Radiative Cooling beneath the Anvil. *J. Atmos. Sci.*, **62**, 2607-2617.

- McCarthy, D., L. Ruthi, and J. Hutton, 2007: The Greensburg, KS, tornado. Preprints, *22nd Conf. on Weather Analysis and Forecasting/18th Conf. on Numerical Weather Prediction*, Park City, UT, Amer. Meteor. Soc., PJ2.4.
- Mead, C. M., and R. L. Thompson, 2011: Environmental characteristics associated with nocturnal significant-tornado events in the central and southern Great Plains. *Electronic J. Severe Storms Meteor.*, **6** (6), 1–35.
- Mesinger, F., and Coauthors, 2006: North American Regional Reanalysis. *Bull. Amer. Meteor. Soc.*, **87**, 343–360.
- Moncrieff, M.W., and M. J. Miller, 1976: The dynamics and simulation of tropical cumulonimbus and squall lines. *Quart. J. Roy. Meteor. Soc.*, **102**, 372-394.
- NWS, 2009: Service Assessment: Super Tuesday Tornado Outbreak of February 5-6, 2008. National Weather Service. [Available online at: http://www.nws.noaa.gov/om/assessments/pdfs/super_tuesday.pdf]
- NWS, 2011: Service Assessment: Joplin, Missouri, Tornado, May 22, 2011. National Weather Service. [Available online at: http://www.nws.noaa.gov/om/assessments/pdfs/Joplin_tornado.pdf]
- NWS, 2011: Service Assessment: The Historic Tornadoes of April 2011. National Weather Service. [Available online at: http://www.nws.noaa.gov/om/assessments/pdfs/historic_tornadoes.pdf]
- Rasmussen, E. N., 2003: Refined supercell and tornado forecast parameters. *Wea. Forecasting*, **18**, 530–535.
- Rochette, S. M., and J. T. Moore, and P. S. Market, 1999: The importance of parcel choice in elevated CAPE computations. *Natl. Wea. Dig.*, **23**, 20-32.
- Saha, S., and Coauthors, 2010: The NCEP climate forecast system reanalysis. *Bull. Amer. Meteor. Soc.*, **91**, 1015–1057.
- Thompson, R. L., R. Edwards, 2000: An Overview of Environmental Conditions and Forecast Implications of the 3 May 1999 Tornado Outbreak. *Wea. Forecasting*, **15**, 682–699.
- Thompson, R. L., R. Edwards, J. A. Hart, K. L. Elmore, and P. Markowski, 2003: Close proximity soundings within supercell environments obtained from the Rapid Update Cycle. *Wea. Forecasting*, **18**, 1243–1261.
- Wakimoto, R. M., and J. W. Wilson, 1989: Non-supercell tornadoes. *Mon. Wea. Rev.*, **117**, 1113-1140.
- Weisman, M. L., and J. B. Klemp, 1982: The dependence of numerically simulated convective storms on vertical wind shear and buoyancy. *Mon. Wea. Rev.*, **110**, 504–520.

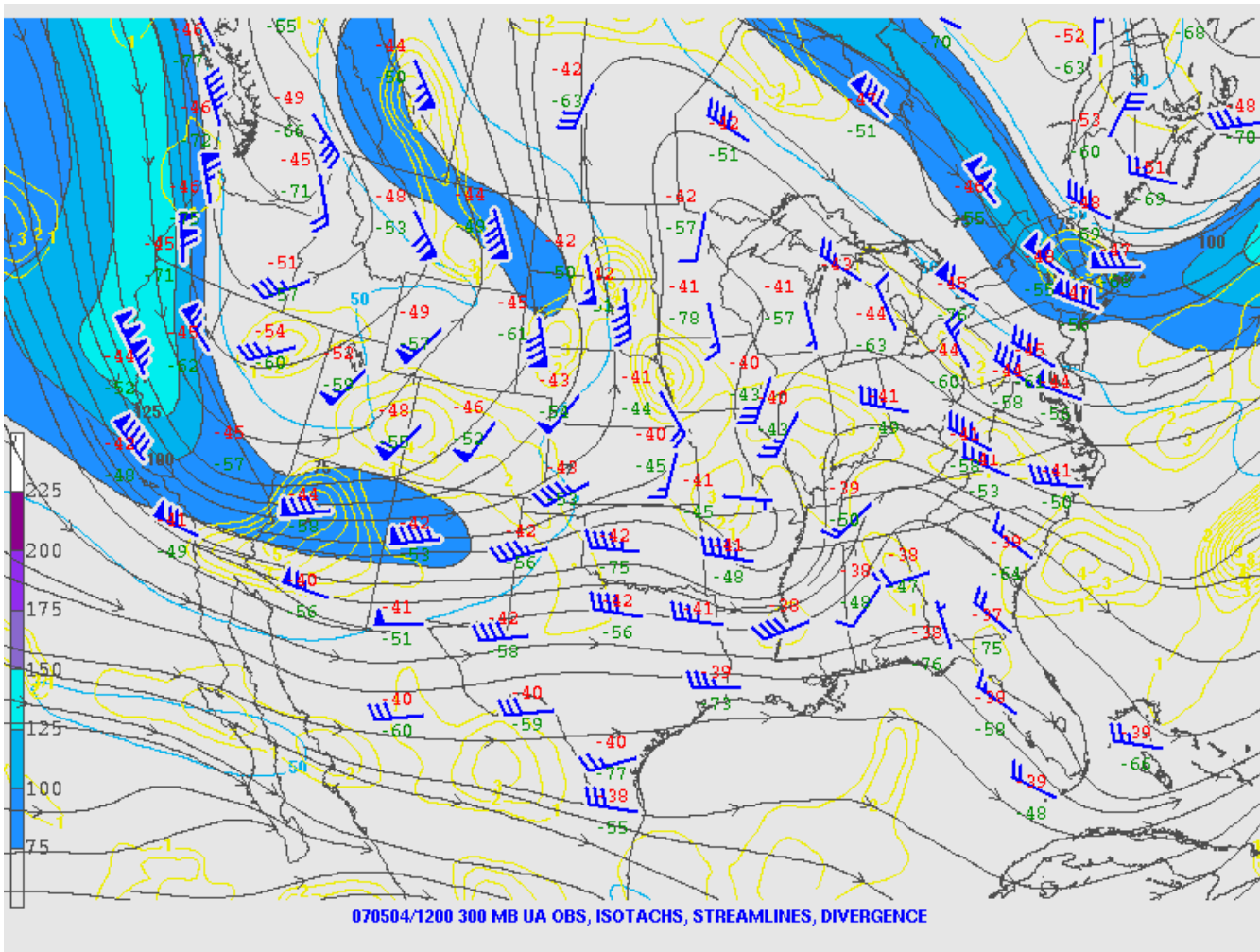


Fig 1. 1200 UTC 4 May 2007 300 hPa observations, streamlines, isotachs (shaded, kts), and divergence (contoured, s^{-1}).

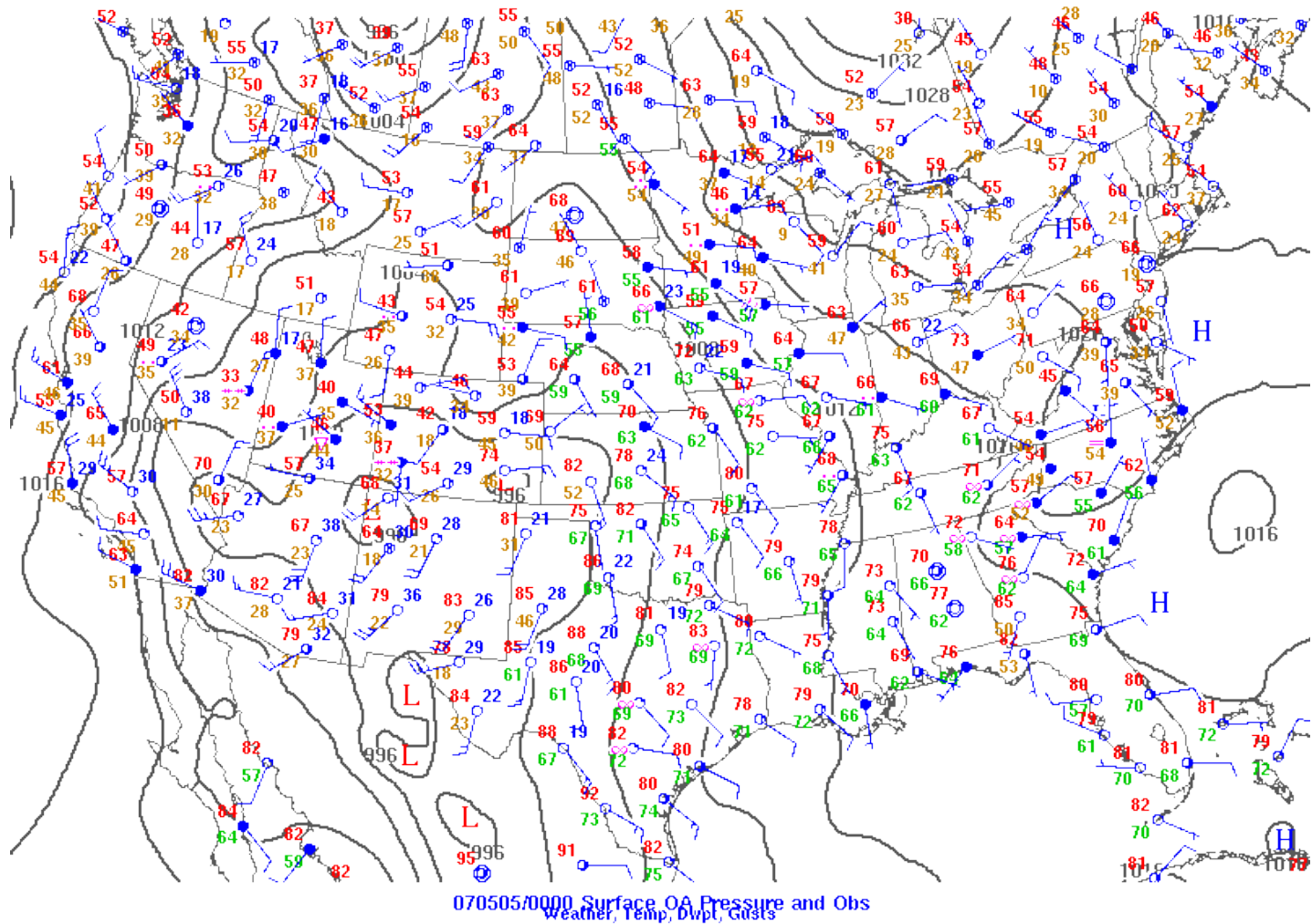


Fig 2. 0000 UTC 5 May 2007 surface observations and pressure analysis.

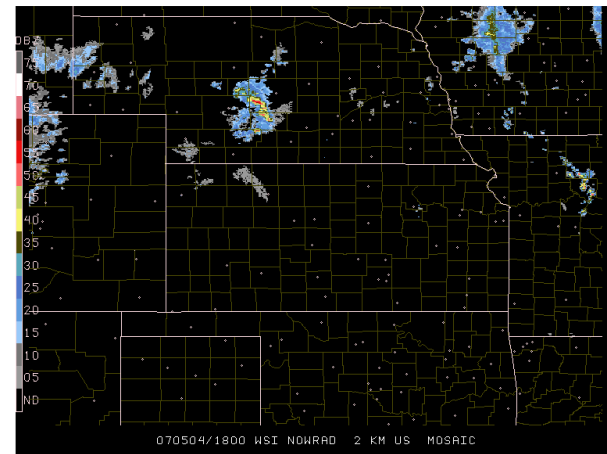
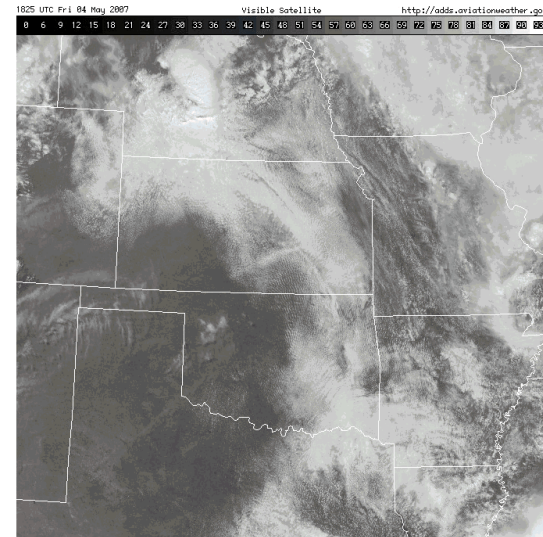
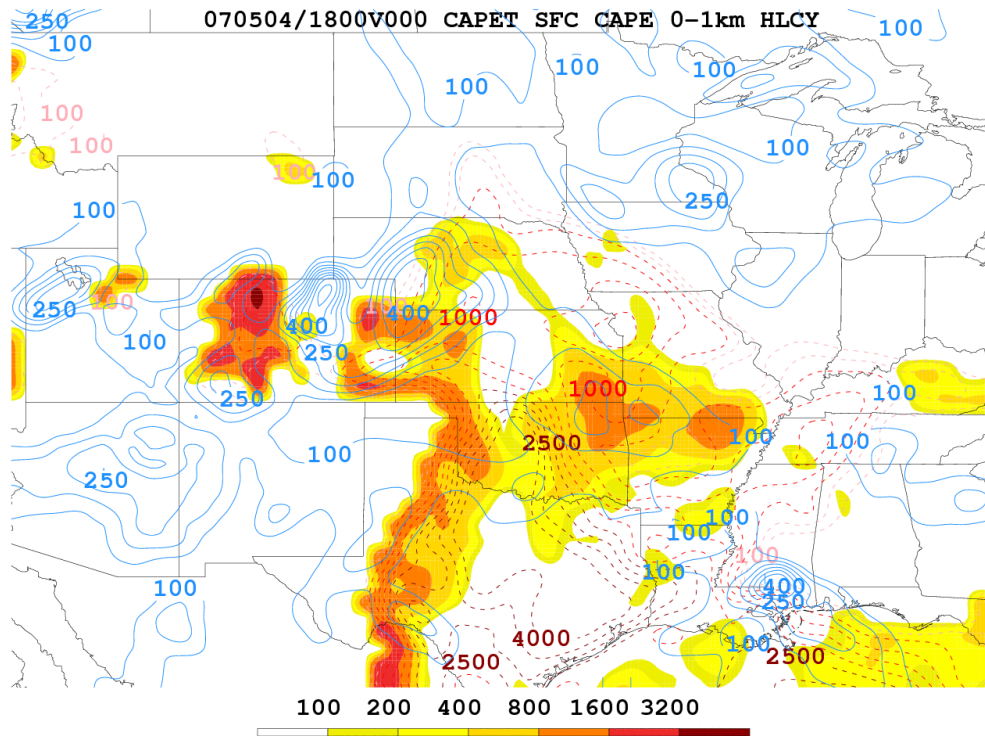


Fig 3. 1800 UTC 4 May 2007 CAPE Tendency Analysis with CAPE tendency (shaded), SBCAPE (hatched), and 0-1 km helicity (contoured). Upper right: 1825 UTC visible satellite imagery. Lower left: 1800 UTC radar composite.

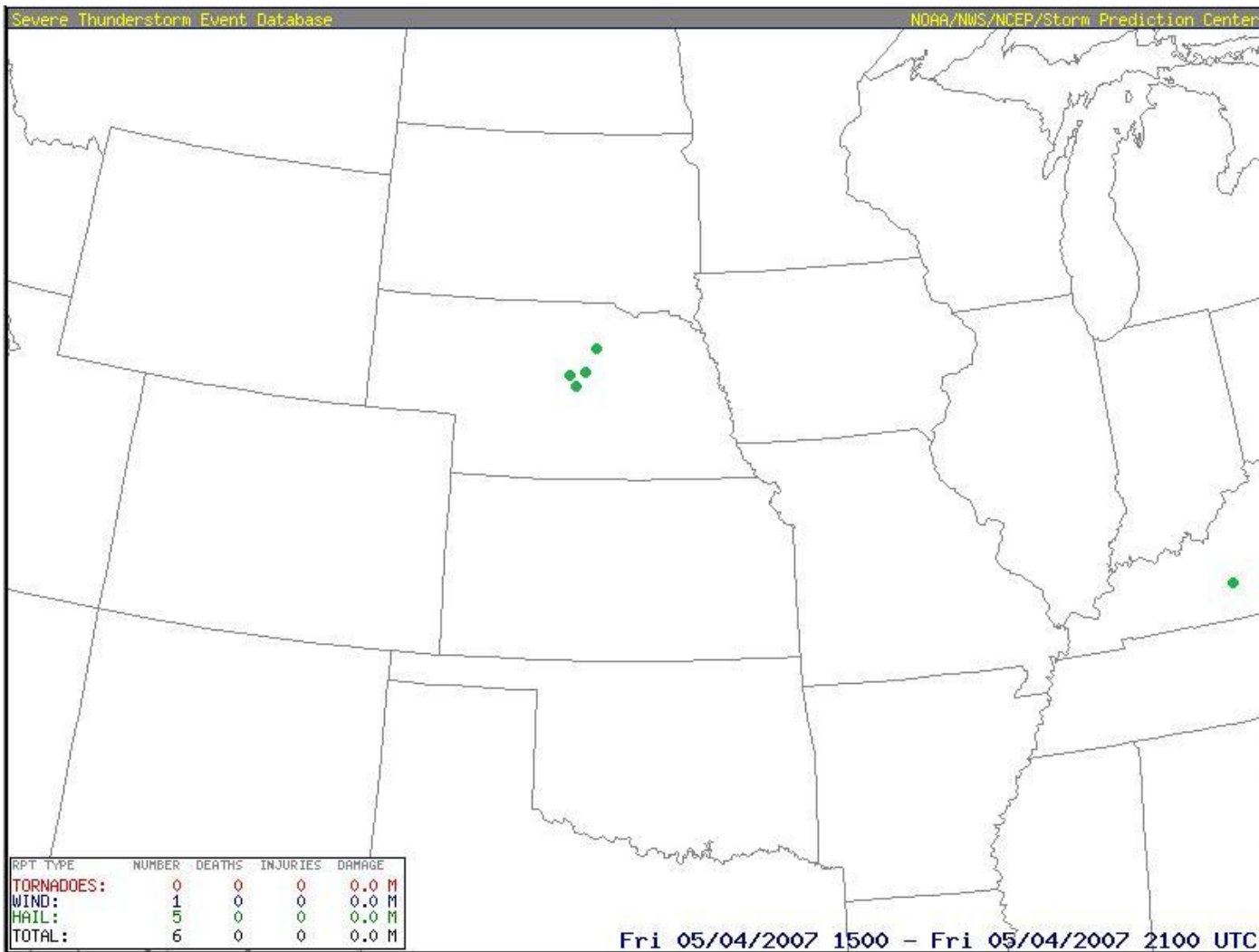


Fig 4. SPC storm reports from 1500 UTC to 2100 UTC 4 May 2007.

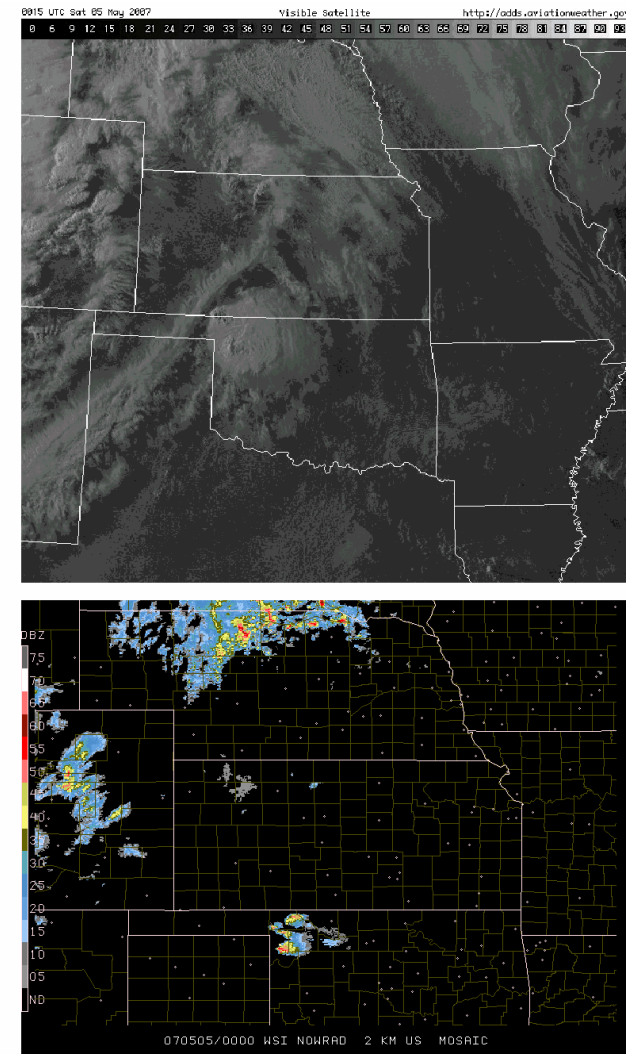
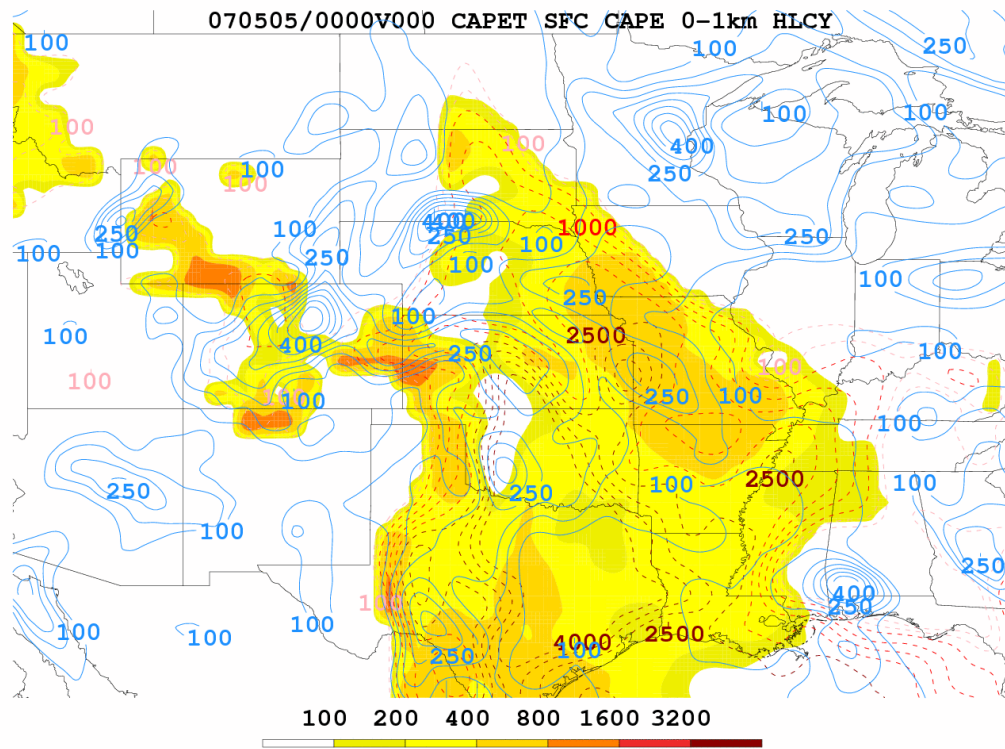


Fig 5. 0000 UTC 5 May 2007 CAPE Tendency Analysis with CAPE tendency (shaded), SBCAPE (hatched), and 0-1 km helicity (contoured). Upper right: 0025 UTC visible satellite imagery. Lower left: 0000 UTC radar composite.

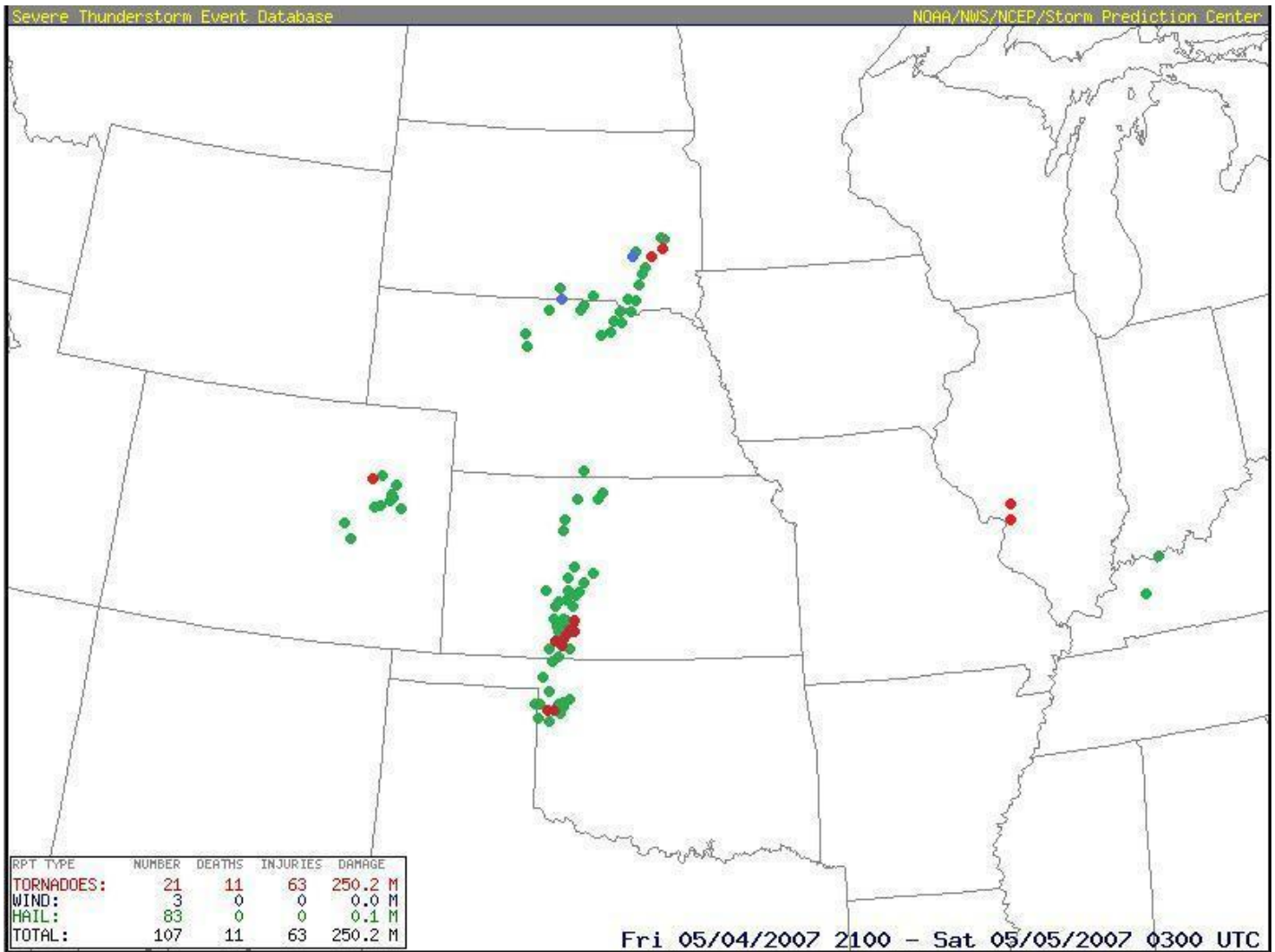


Fig 6. SPC storm reports from 2100 UTC 4 May to 0300 UTC 5 May.

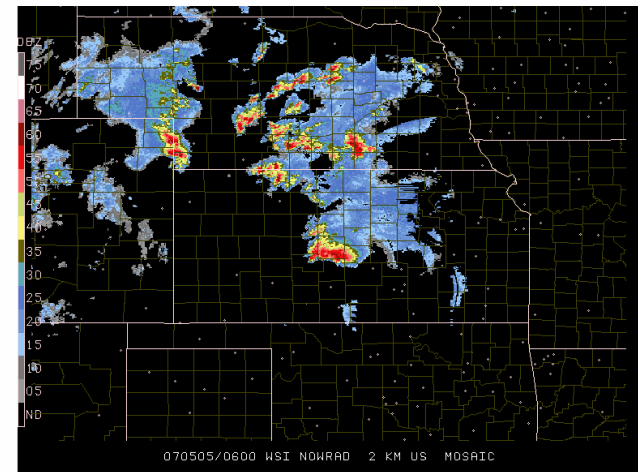
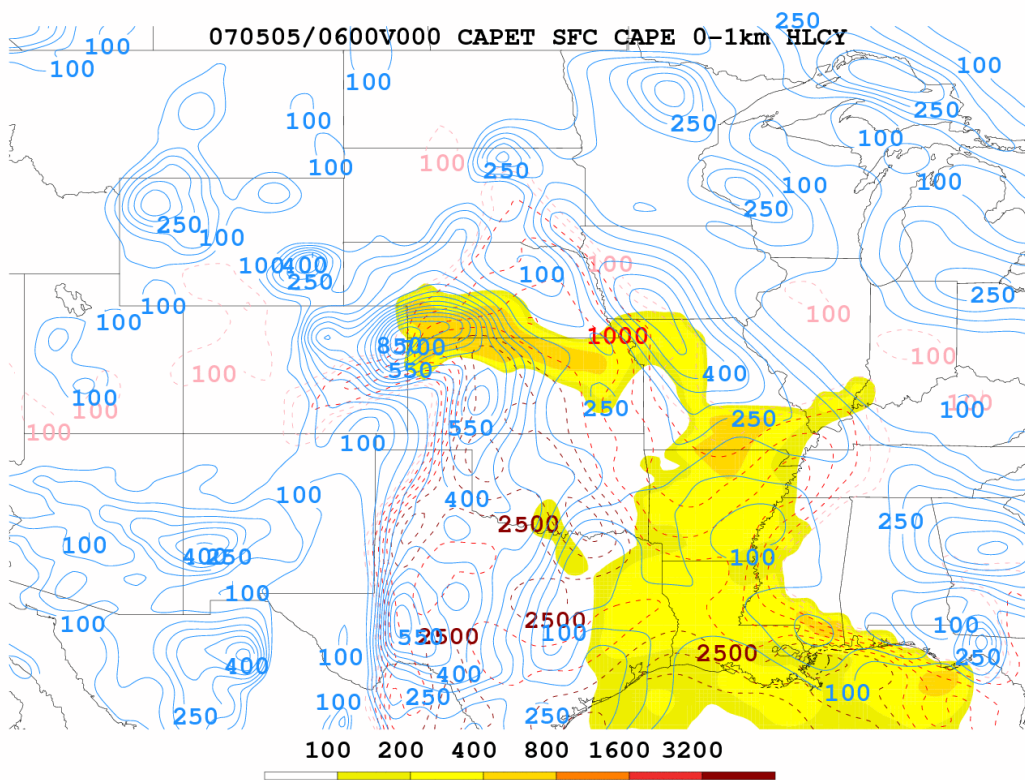


Fig 7. 0600 UTC 5 May 2007 CAPE Tendency Analysis with CAPE tendency (shaded), SBCAPE (hatched), and 0-1 km helicity (contoured). Right side: 0600 UTC radar composite.

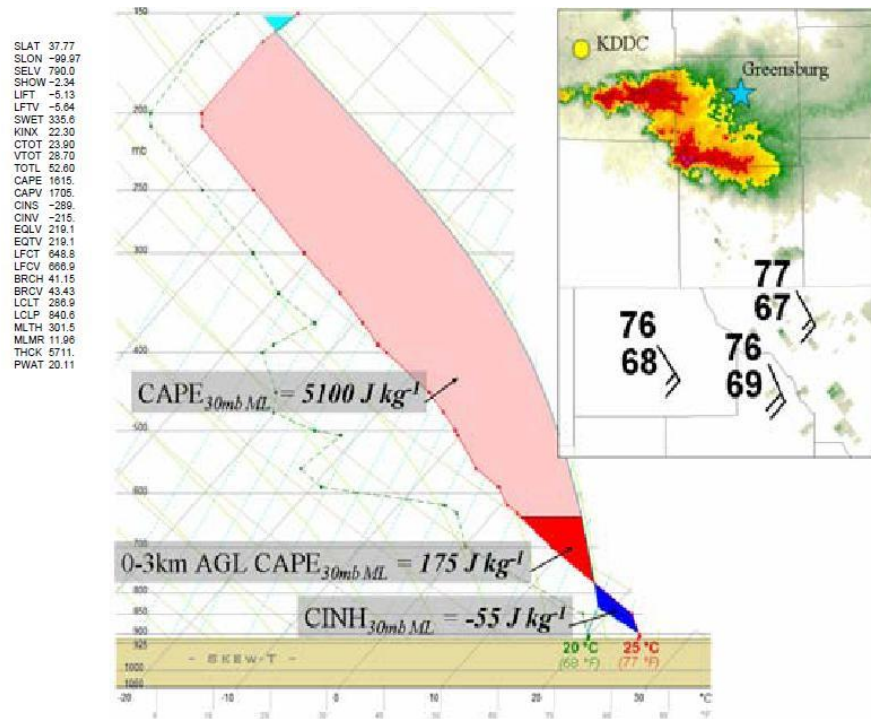
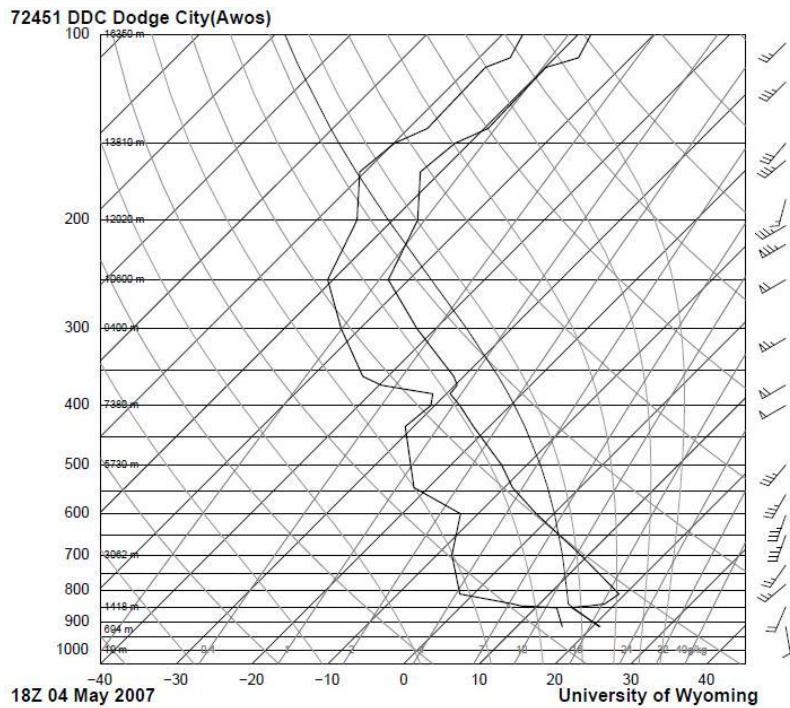


Fig 8. Left: 1800 UTC 4 May 2007 Skew-T log-P diagram from Dodge City, Kansas (DDC) indicating CAPE of 1615 Jkg⁻¹. Right: Skew-T log-P diagram of modified 0000 KDDC-RAOB representing Greensburg storm-inflow thermodynamic characteristics. Oklahoma mesonet observations at 0200 plotted in the upper-right inset and used to modify the 0000 sounding up to ~ 850 mb. KDDC WSR-88D 0.9° reflectivity including supercell south of Greensburg at 0205 also included. [From Fig. 4 of Lemon and Umscheid, 2008]

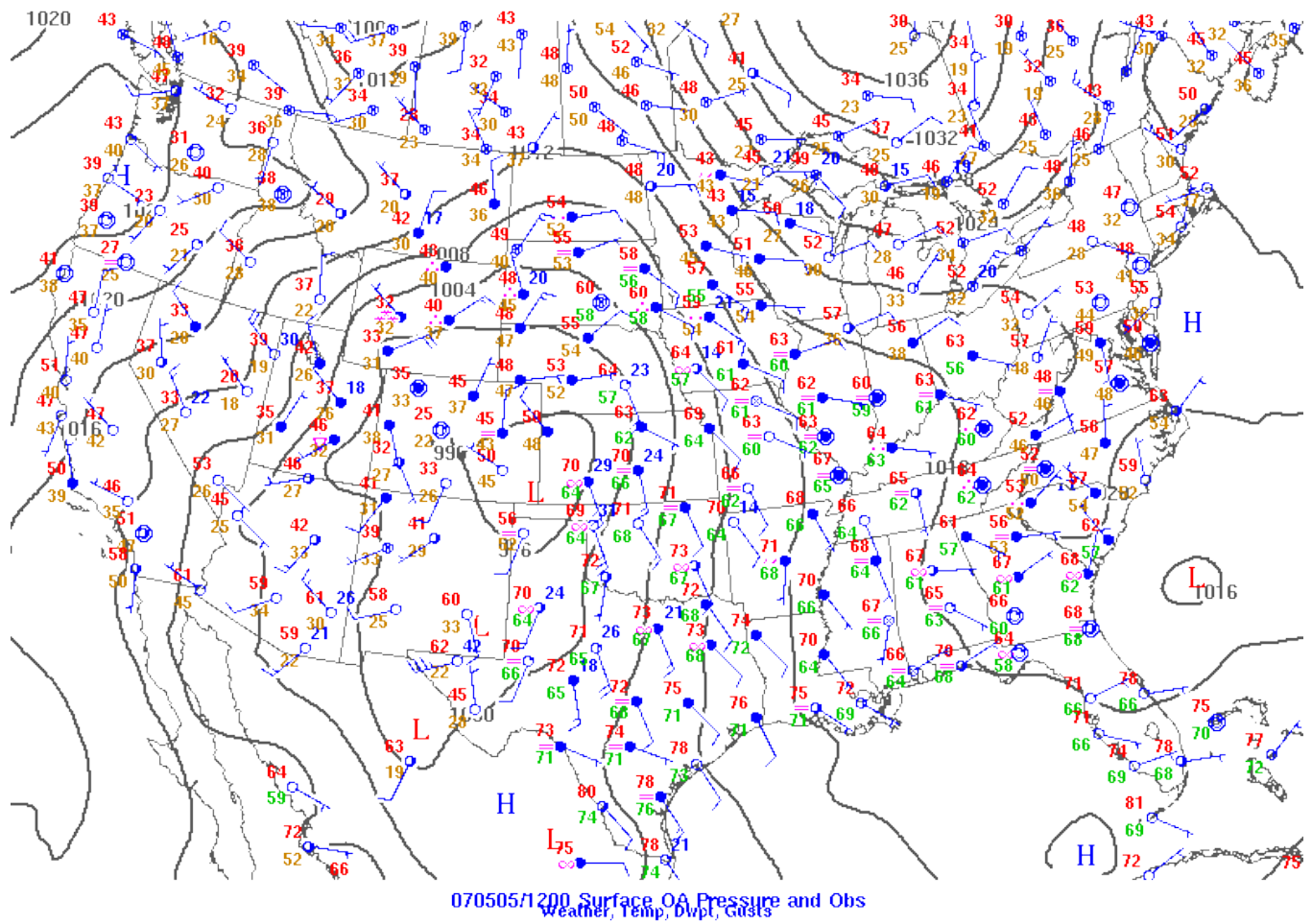


Fig 9. 1200 UTC 5 May 2007 surface observations and pressure analysis.

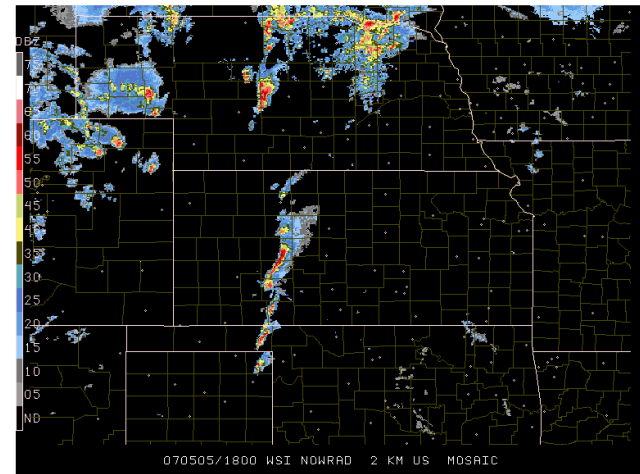
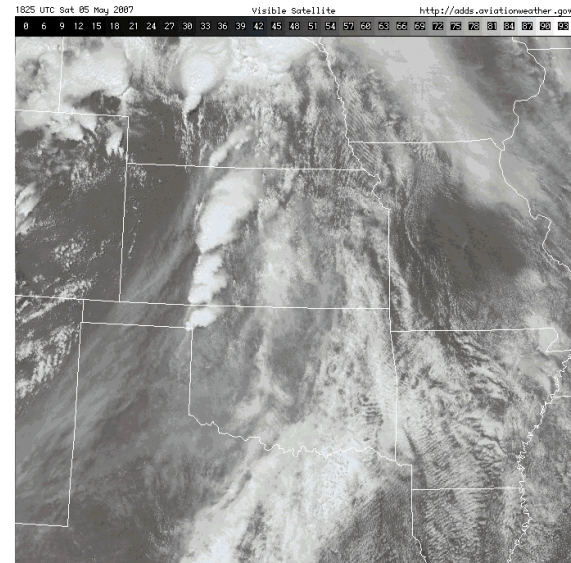
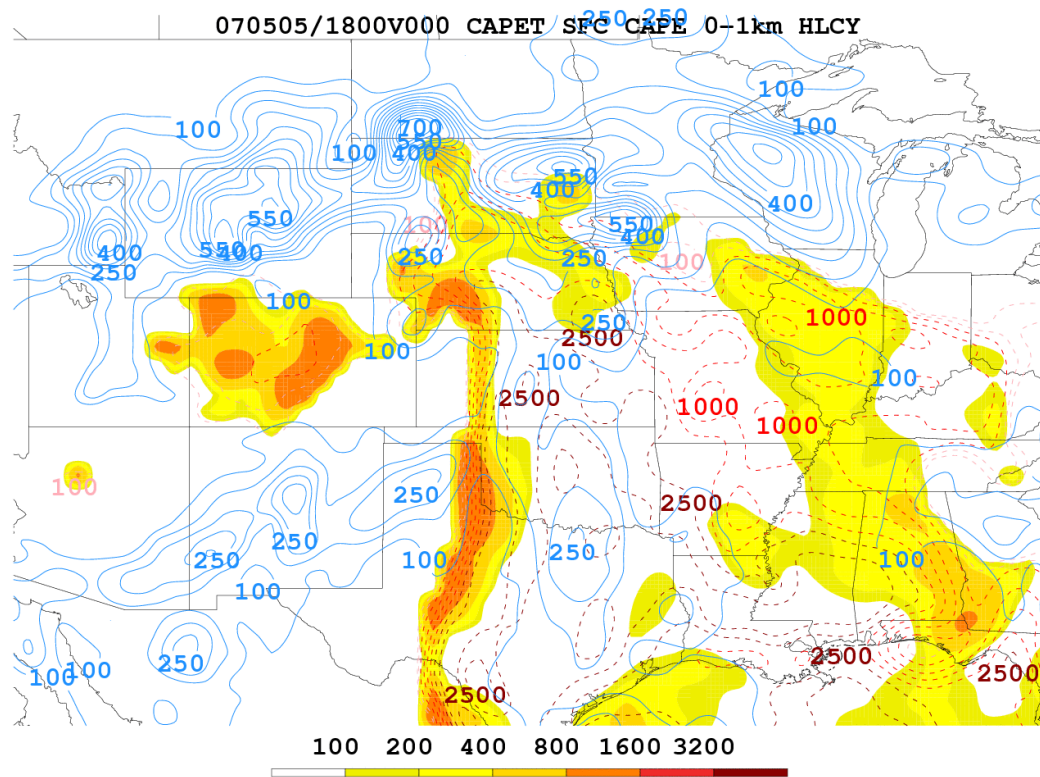


Fig 11. 1800 UTC 5 May 2007 CAPE Tendency Analysis with CAPE tendency (shaded), SBCAPE (hatched), and 0-1 km helicity (contoured). Upper right: 1825 UTC visible satellite imagery. Lower left: 1800 UTC radar composite.

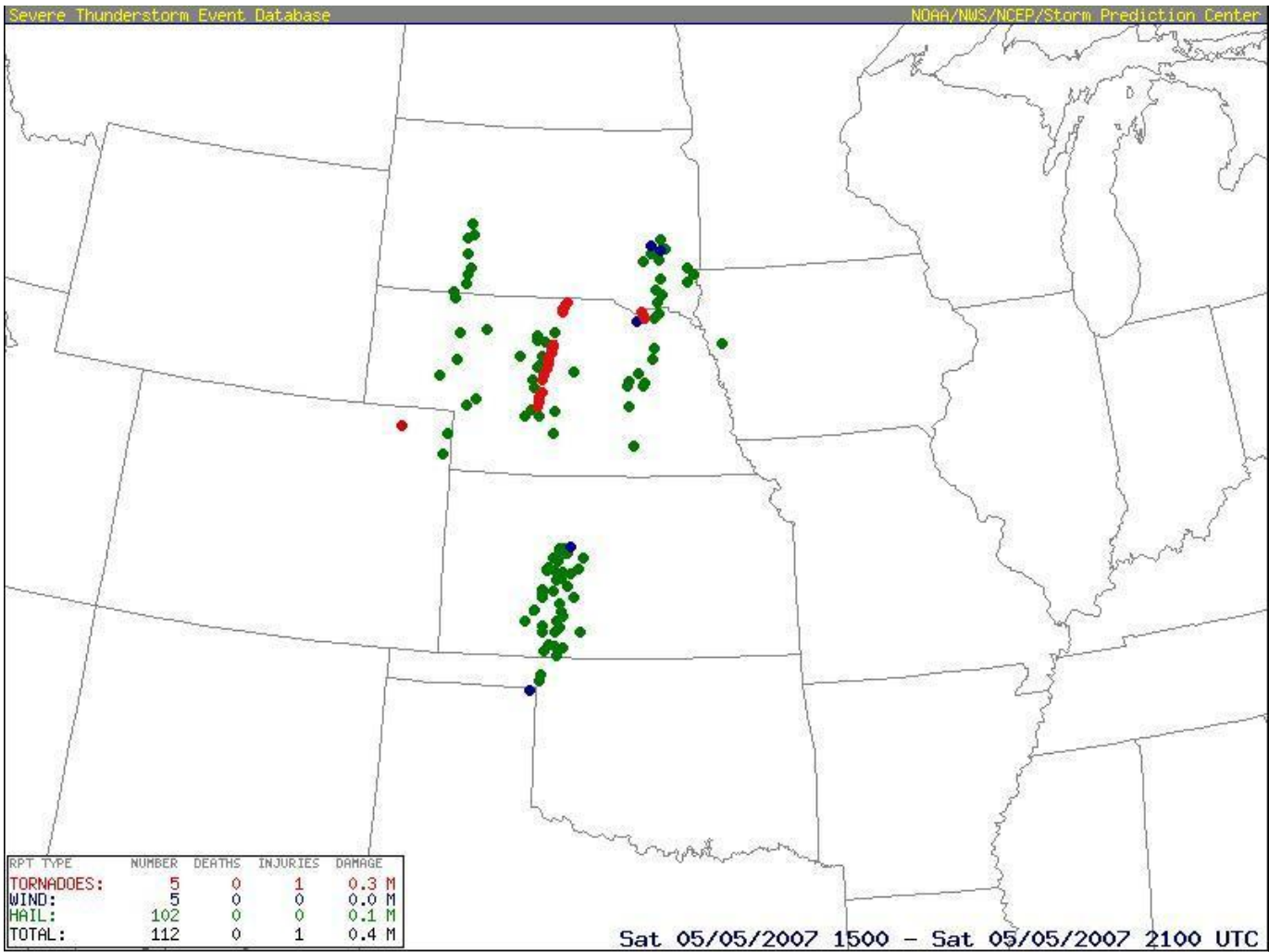


Fig 12. SPC storm reports from 1500 UTC to 2100 UTC 5 May.

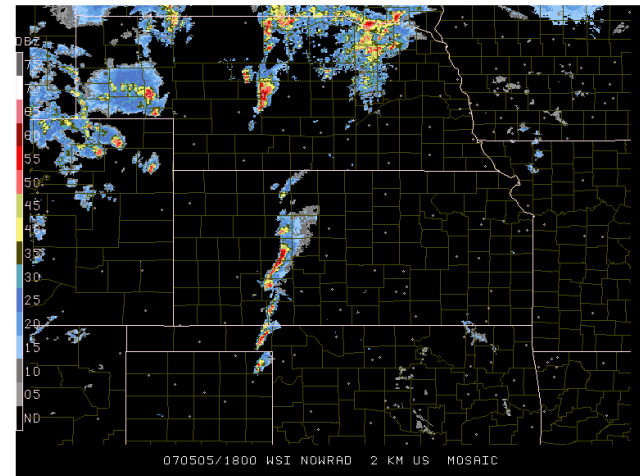
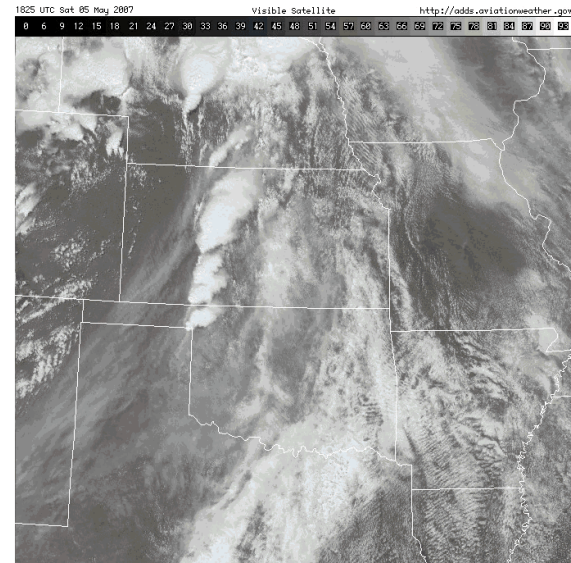
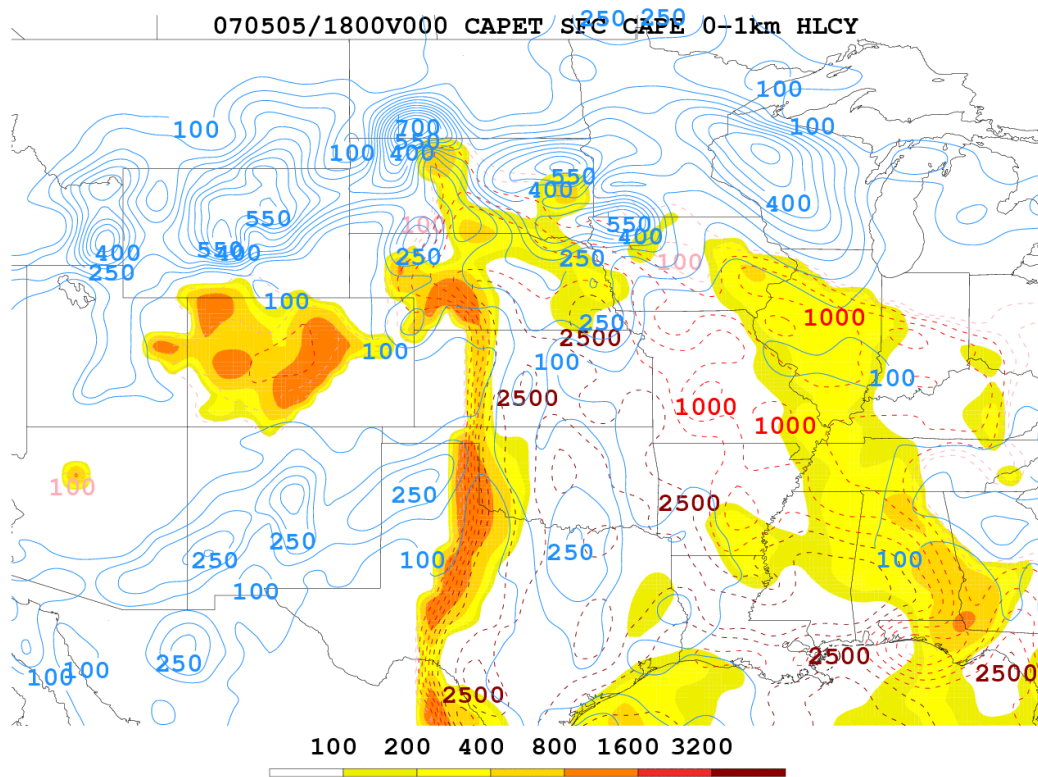


Fig 13. 0000 UTC 6 May 2007 CAPE Tendency Analysis with CAPE tendency (shaded), SBCAPE (hatched), and 0-1 km helicity (contoured). Upper right: 0025 UTC visible satellite imagery. Lower left: 0000 UTC radar composite.

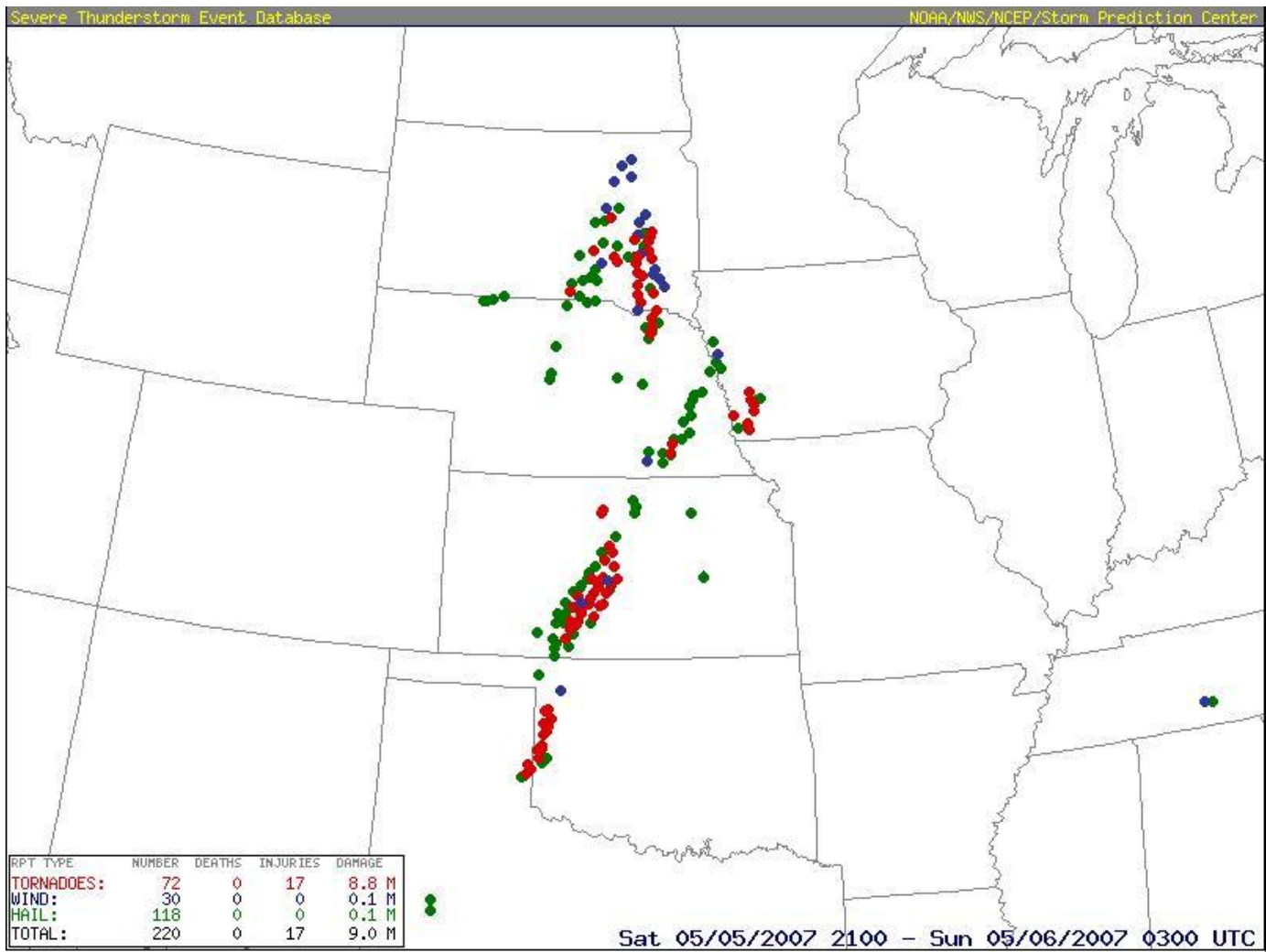


Fig 14. SPC storm reports 2100 UTC 5 May to 0300 UTC 6 May.

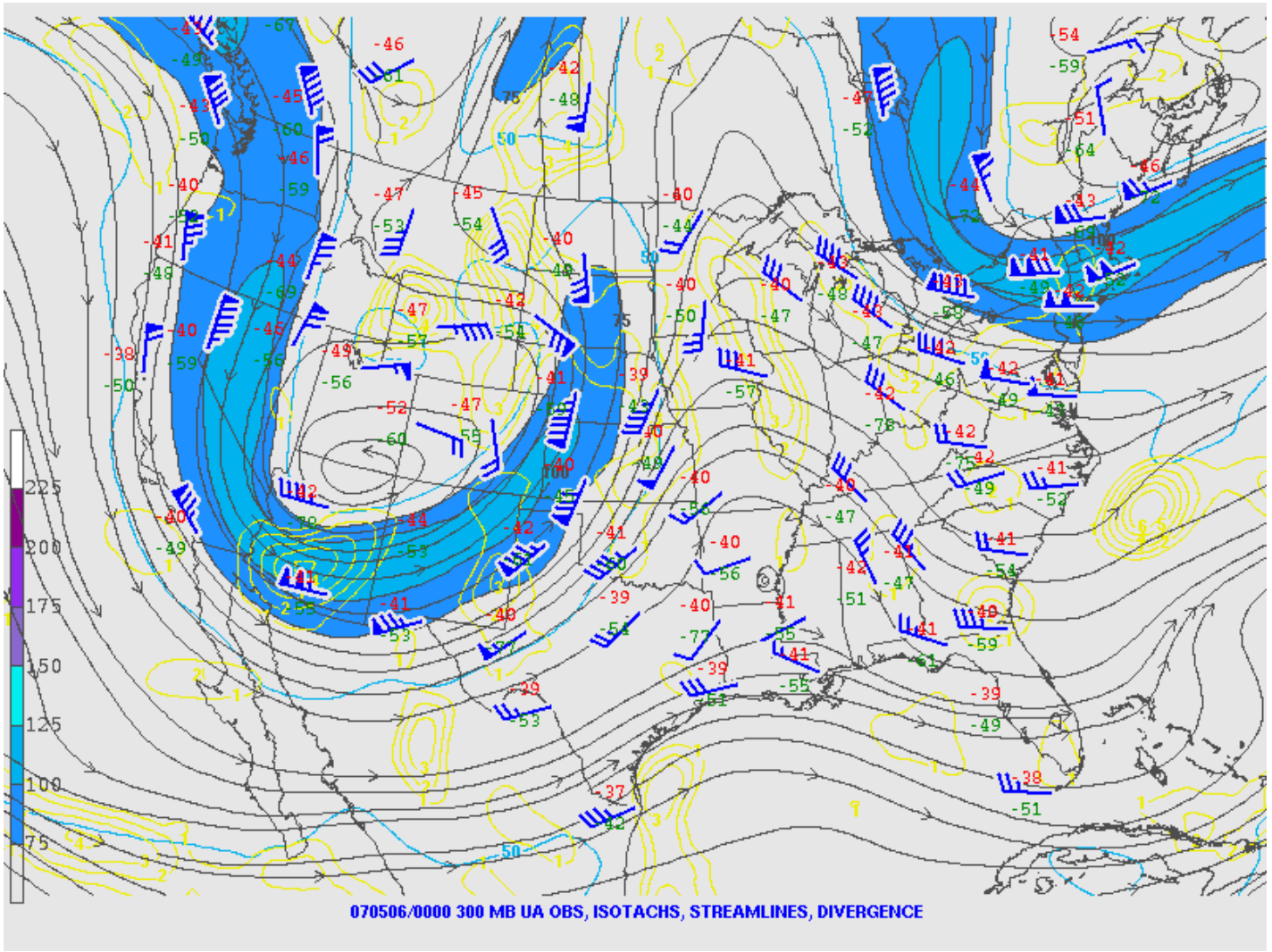


Fig 15. 0000 UTC 6 May 2007 300 hPa observations, streamlines, isotachs (shaded, kts), and divergence (contoured, s^{-1}).

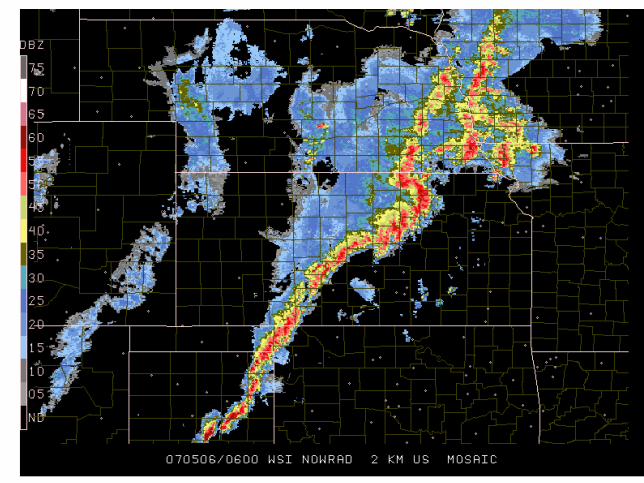
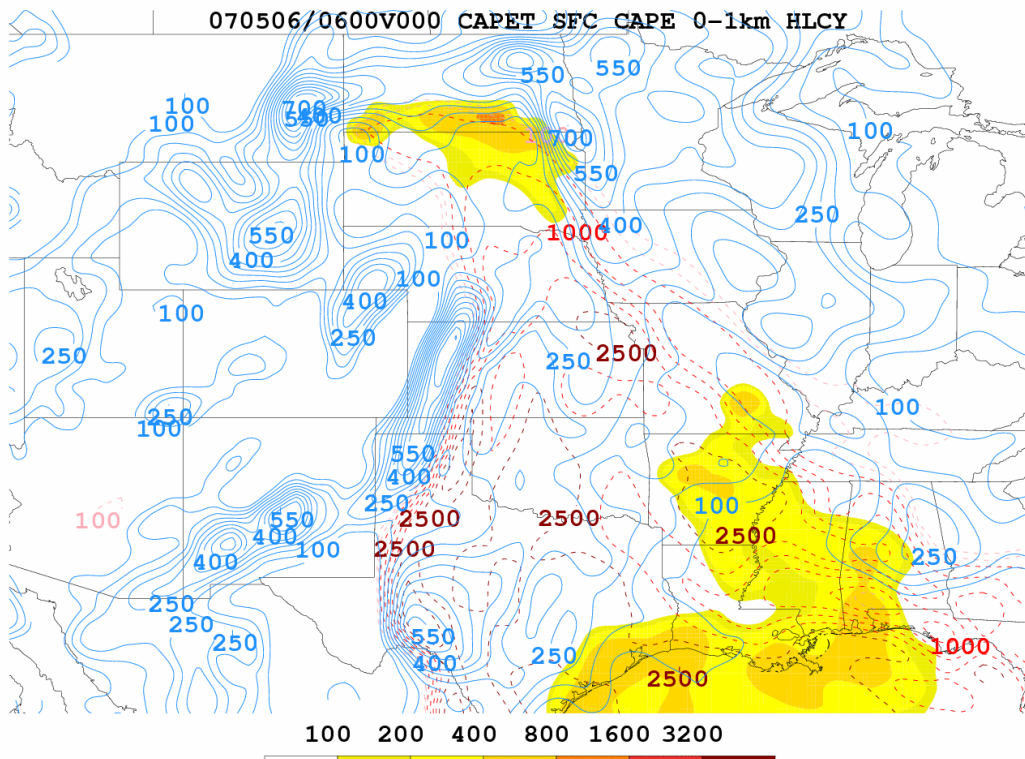


Fig 16. 0600 UTC 6 May 2007 CAPE Tendency Analysis with CAPE tendency (shaded), SBCAPE (hatched), and 0-1 km helicity (contoured). Right Side: 0600 UTC radar composite.

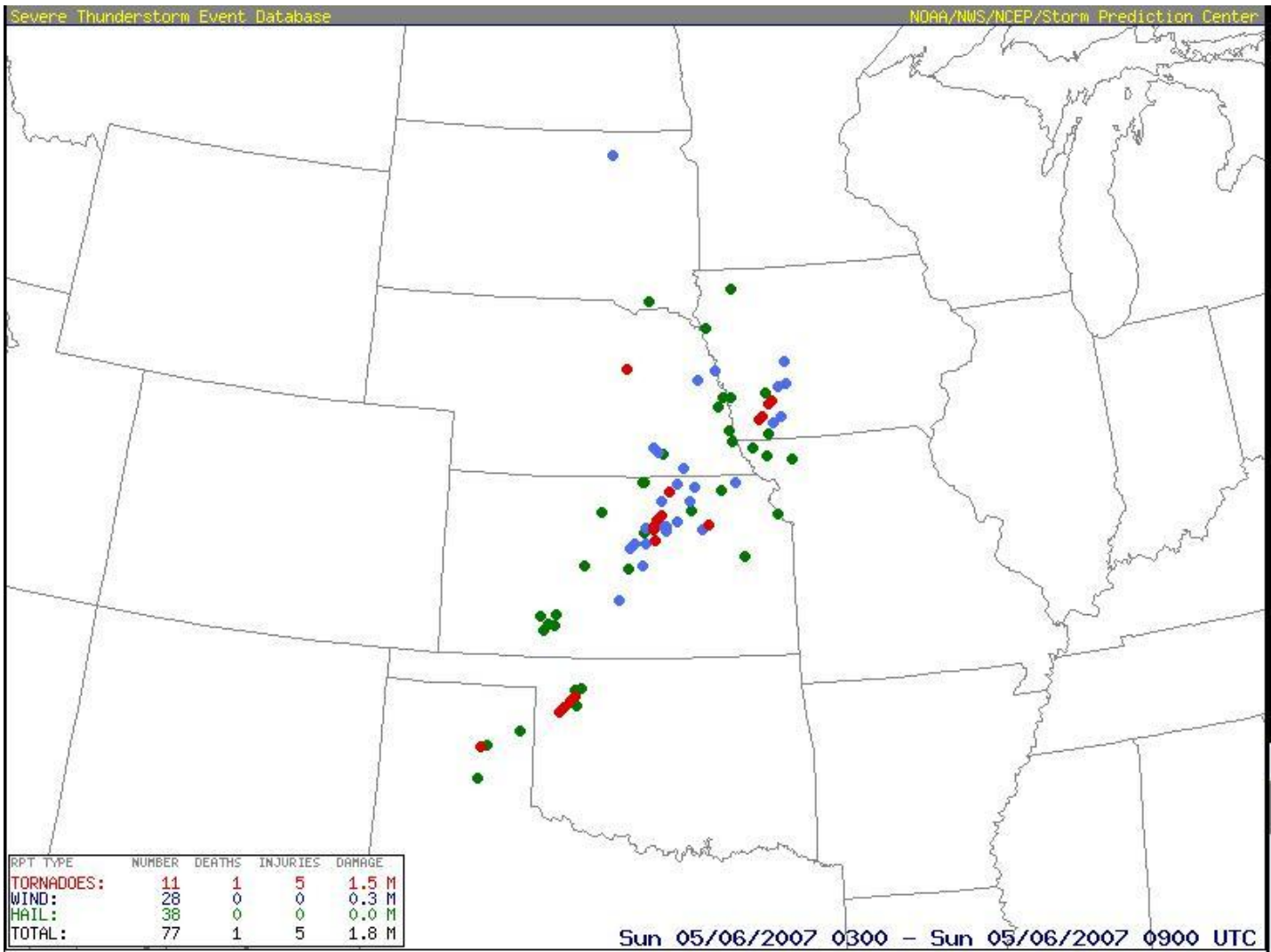


Fig 17. SPC storm reports from 0300 UTC to 0900 UTC 6 May.

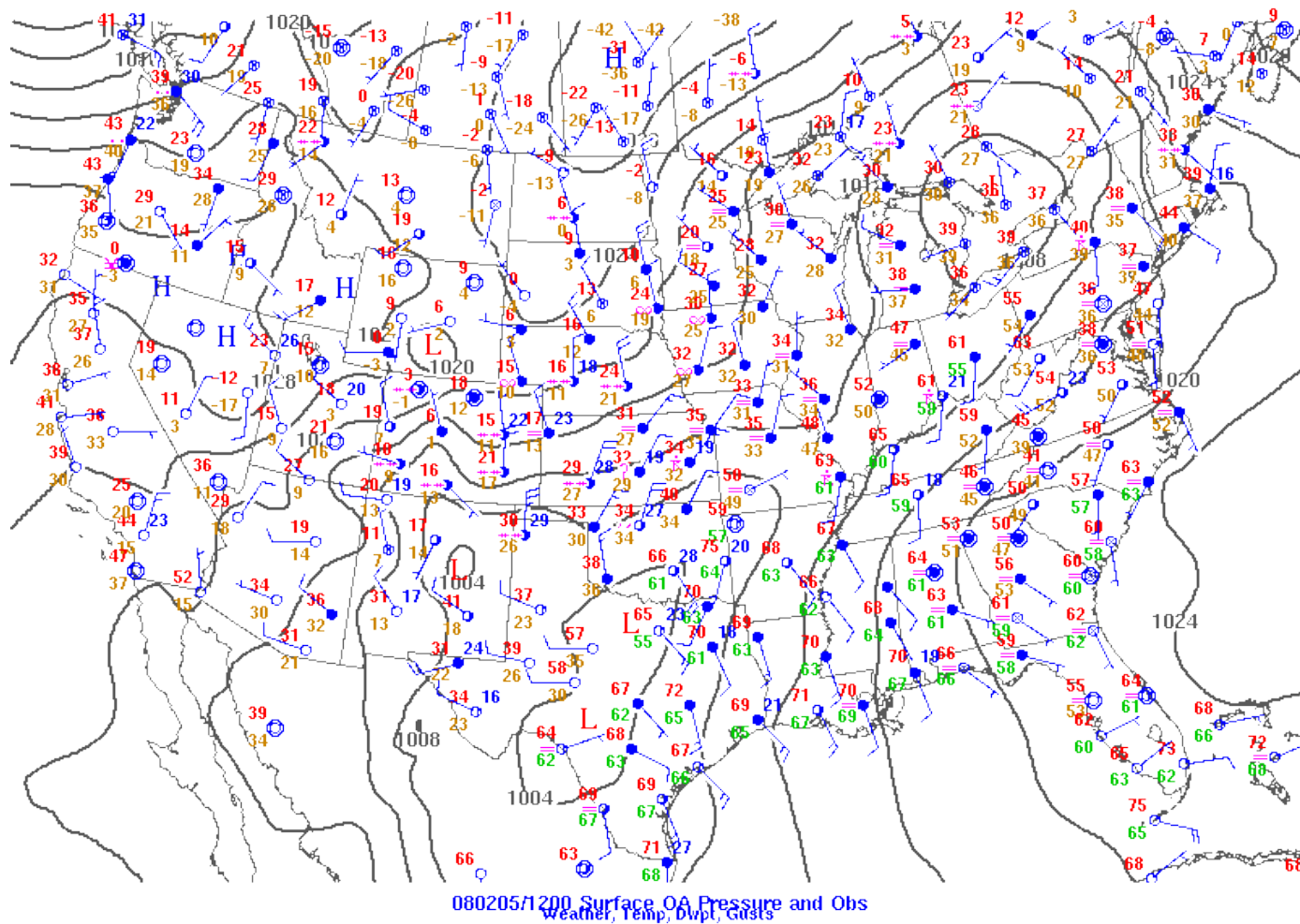


Fig 18. 1200 UTC 5 February 2008 surface observations and pressure analysis.

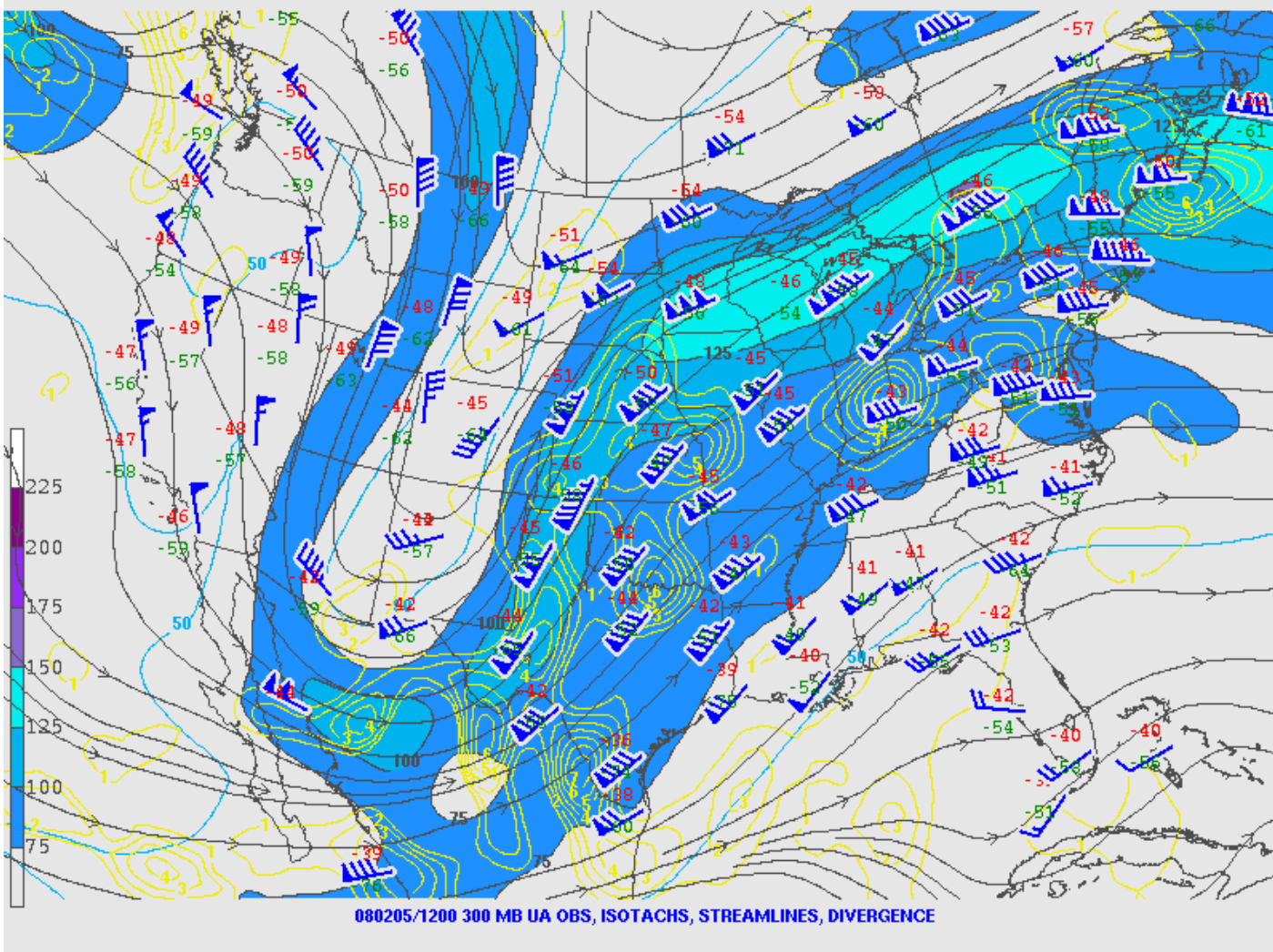


Fig 19: 1200 UTC 5 February 2008 300 hPa observations, streamlines, isotachs (shaded, kts), and divergence (contoured, s^{-1}).

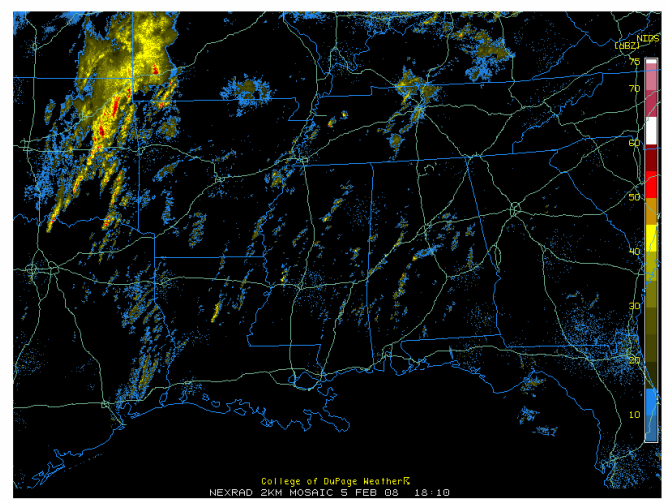
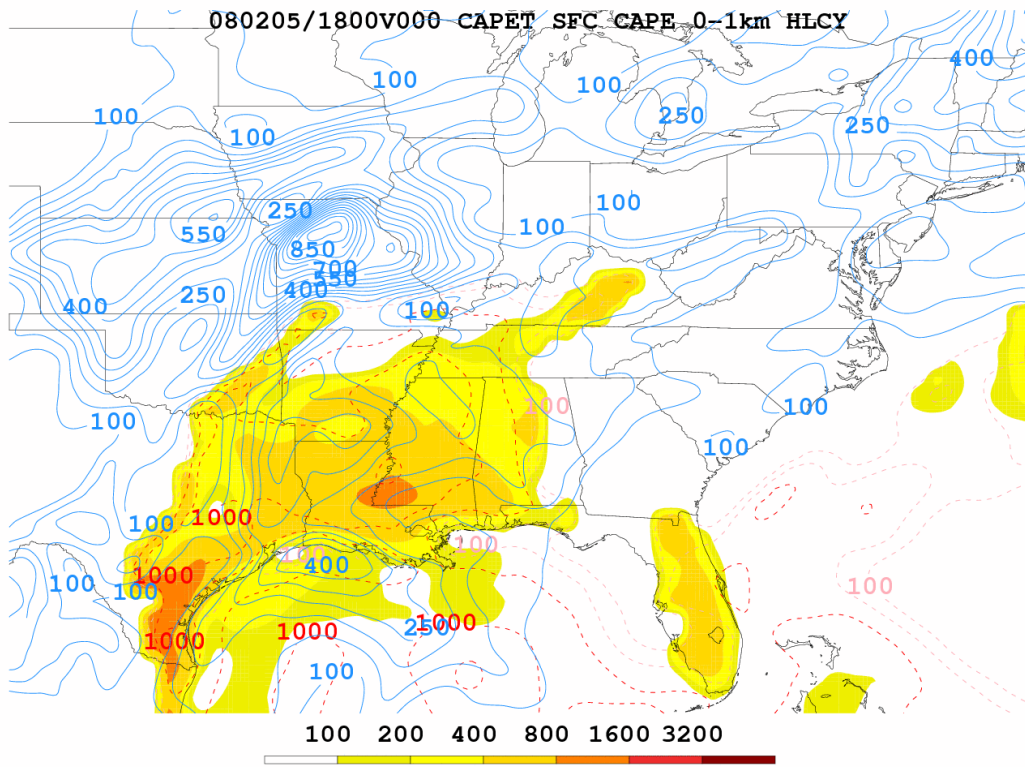


Fig 20. 1800 UTC 5 February 2008 CAPE Tendency Analysis with CAPE tendency (shaded), SBCAPE (hatched), and 0-1 km helicity (contoured). Right Side: 1800 UTC radar composite.

72340 LZK North Little Rock

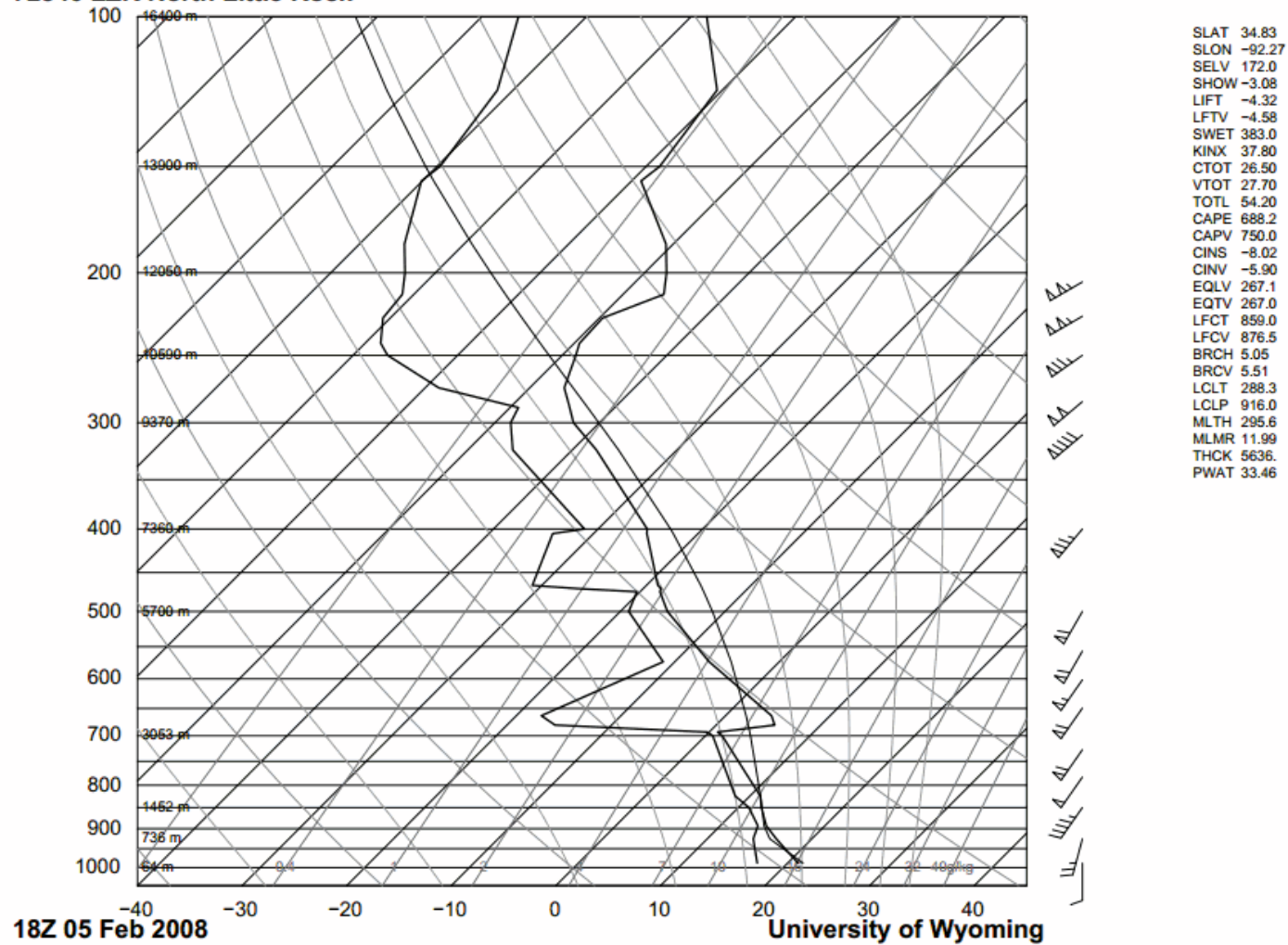


Fig 21: 1800 UTC 5 February 2008 Skew-T log-P diagram from Little Rock, Arkansas indicating winds greater than 50 kts above 800 hPa and a strong temperature inversion above 700 hPa.

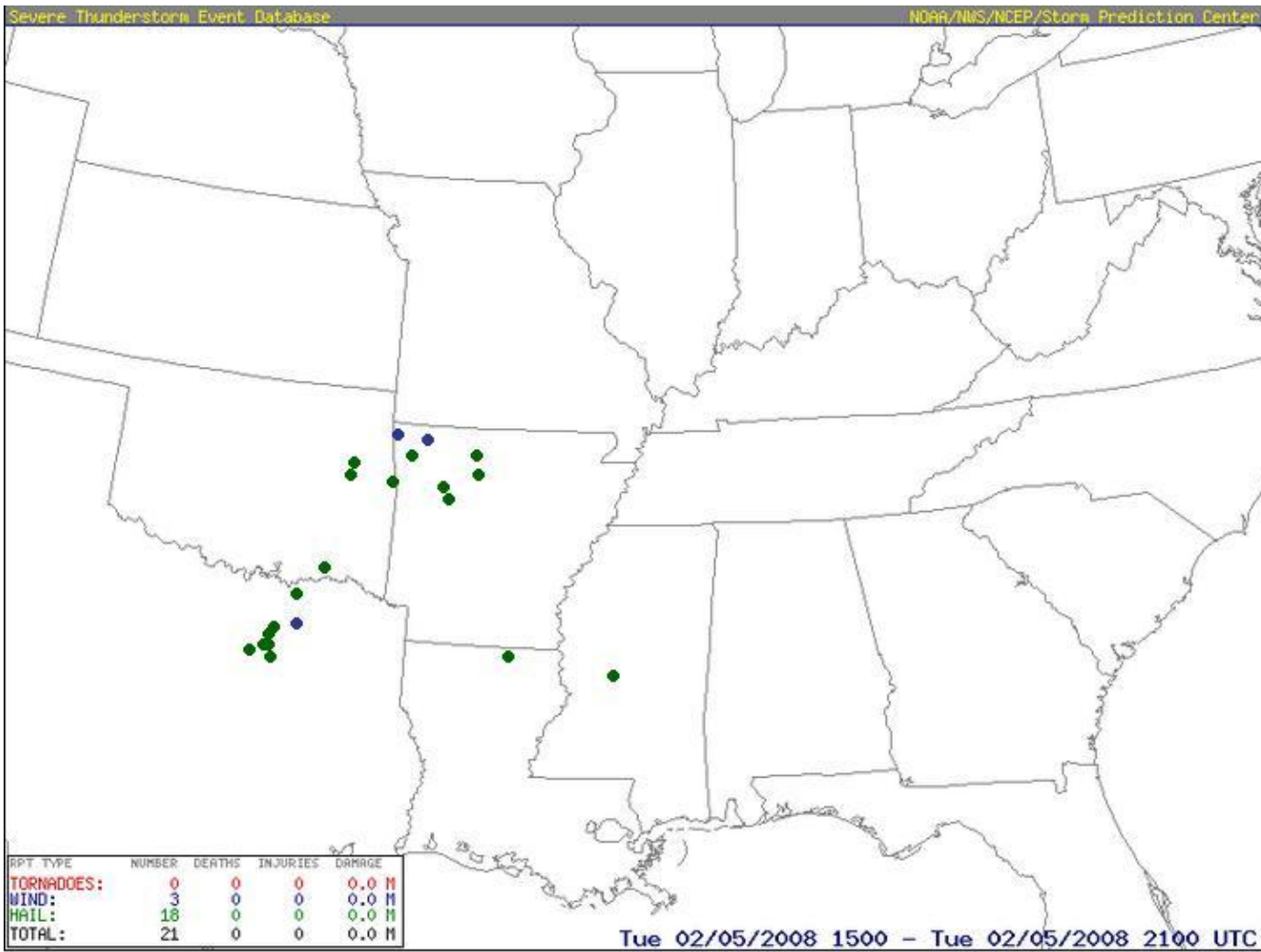


Fig 22. SPC storm reports from 1500 UTC to 2100 UTC 5 February 2008.

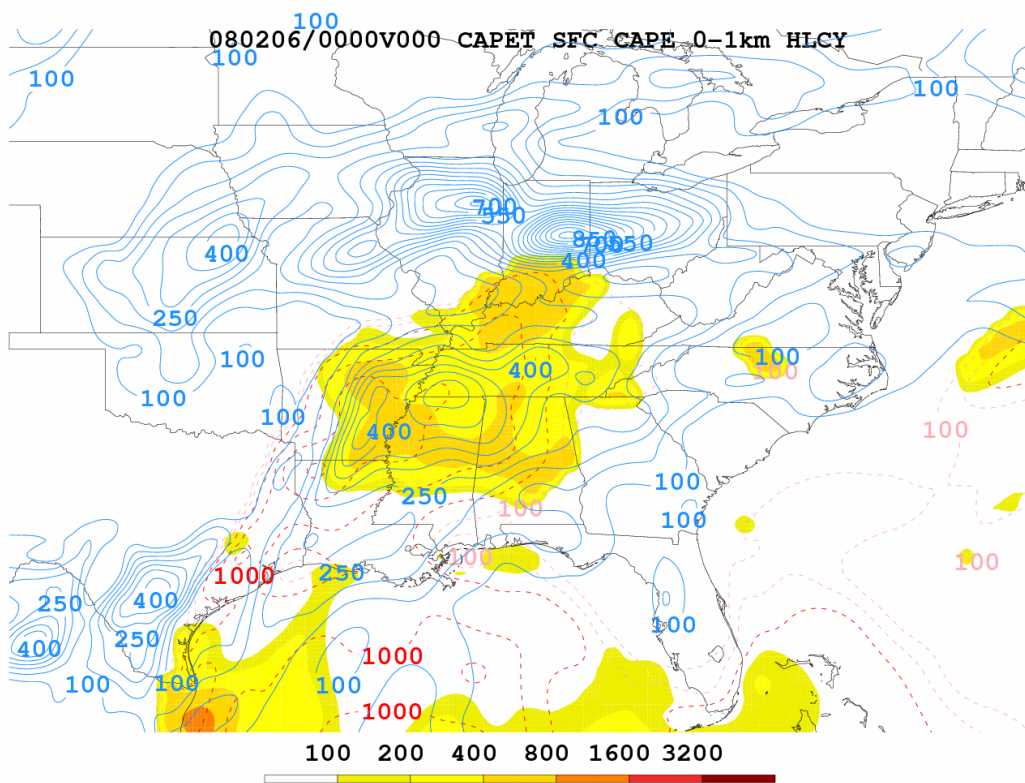


Fig 23. 0000 UTC 6 February 2008 CAPE Tendency Analysis with CAPE tendency (shaded), SBCAPE (hatched), and 0-1 km helicity (contoured). Right Side: 0000 UTC radar composite.

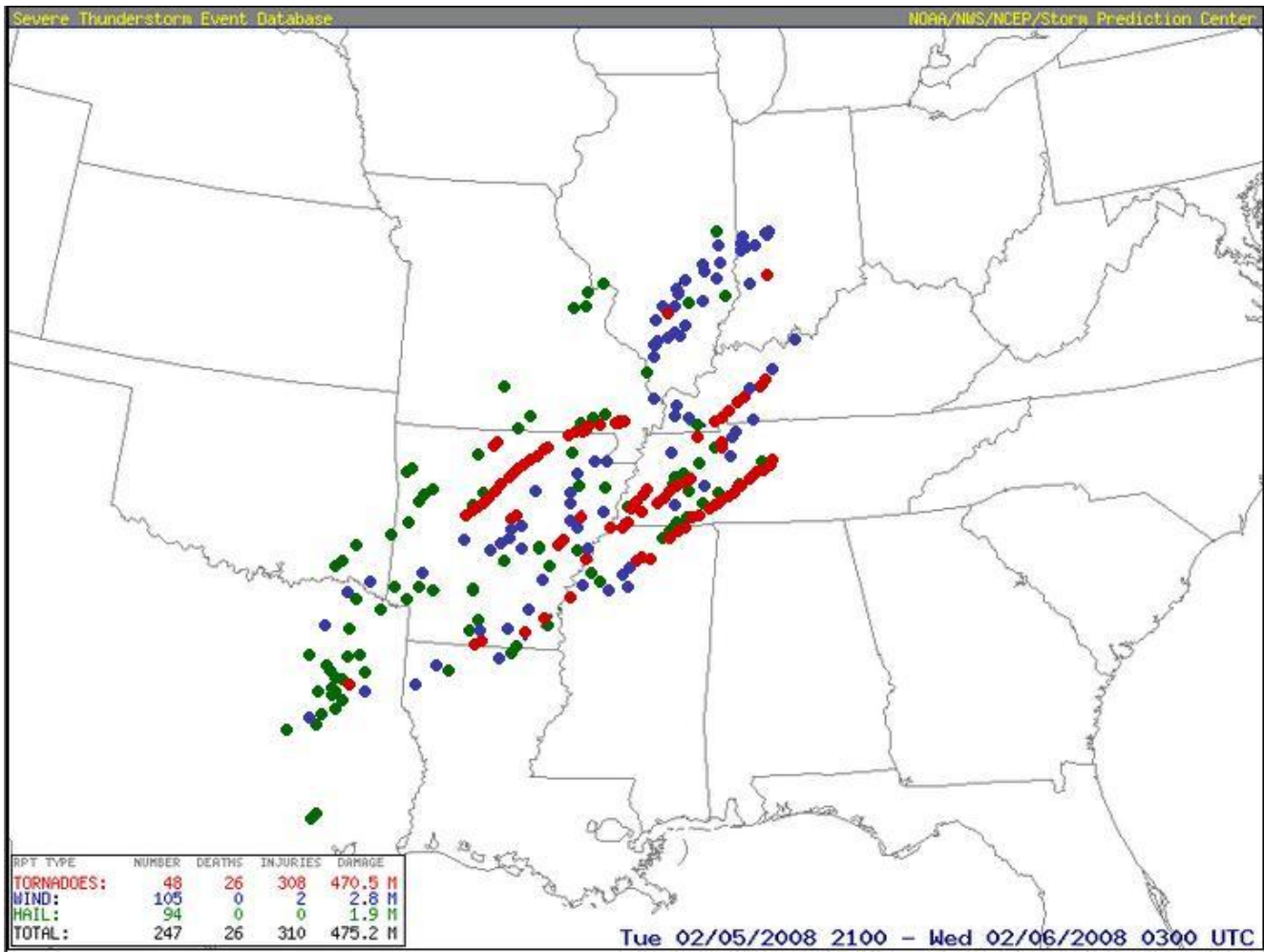


Fig 24. SPC storm reports from 2100 UTC 5 February 2008 to 0300 UTC 6 February 2008.

72327 BNA Nashville

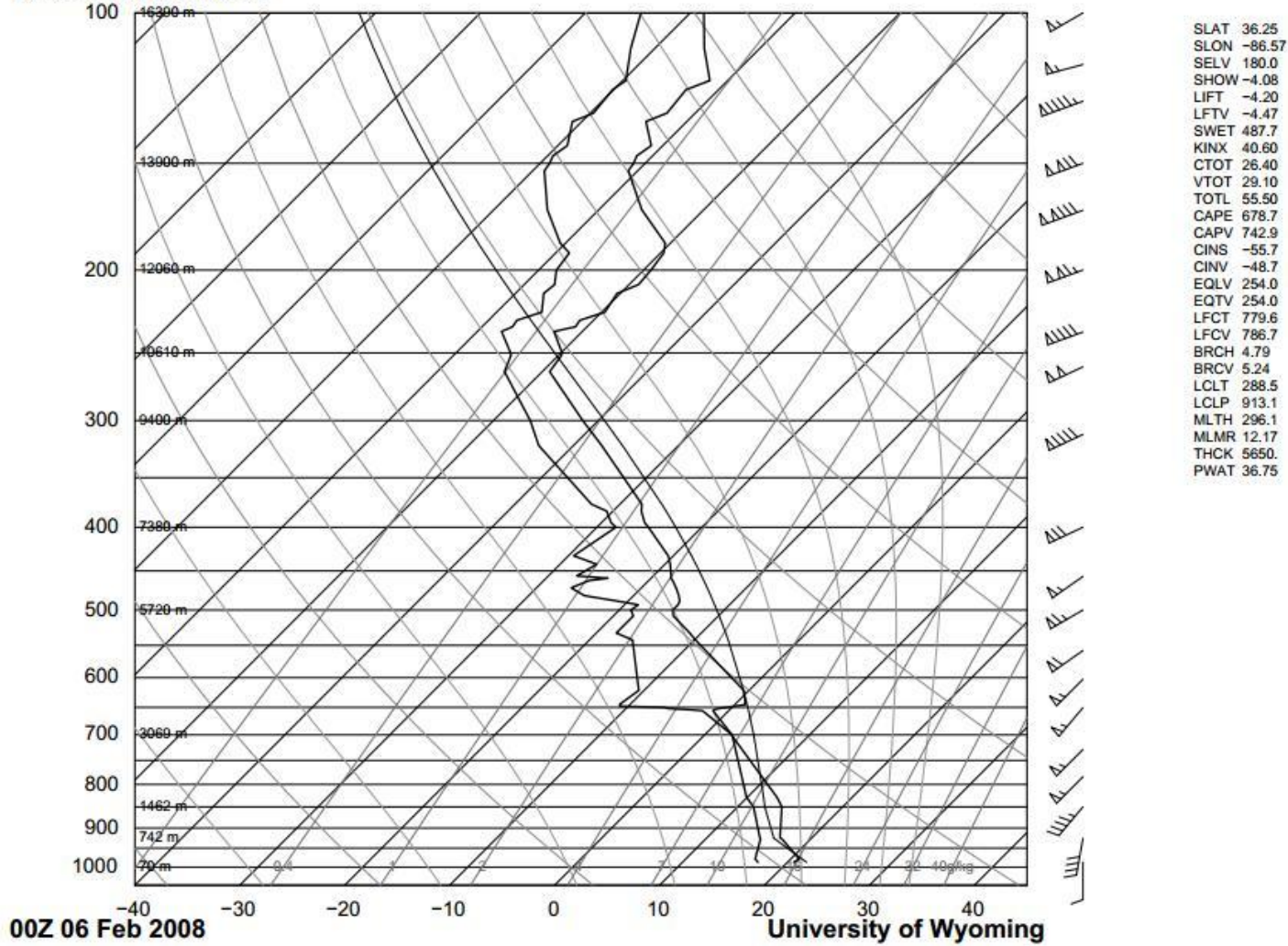


Fig 26. 0000 UTC 6 February 2008 Skew-T log-P diagram from Nashville, Tennessee.

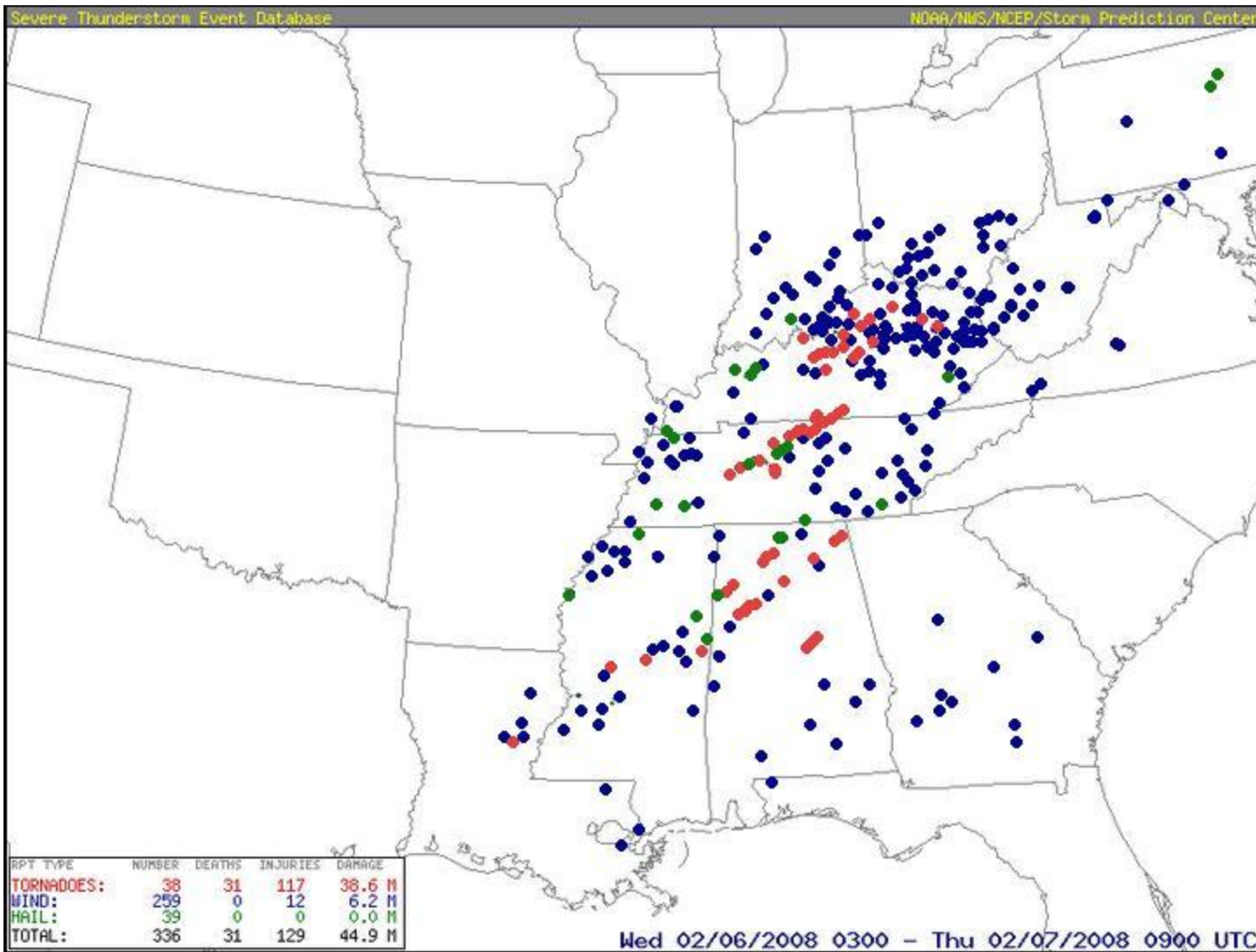


Fig 26: SPC storm reports from 0300 UTC to 0900 UTC 6 February 2008.

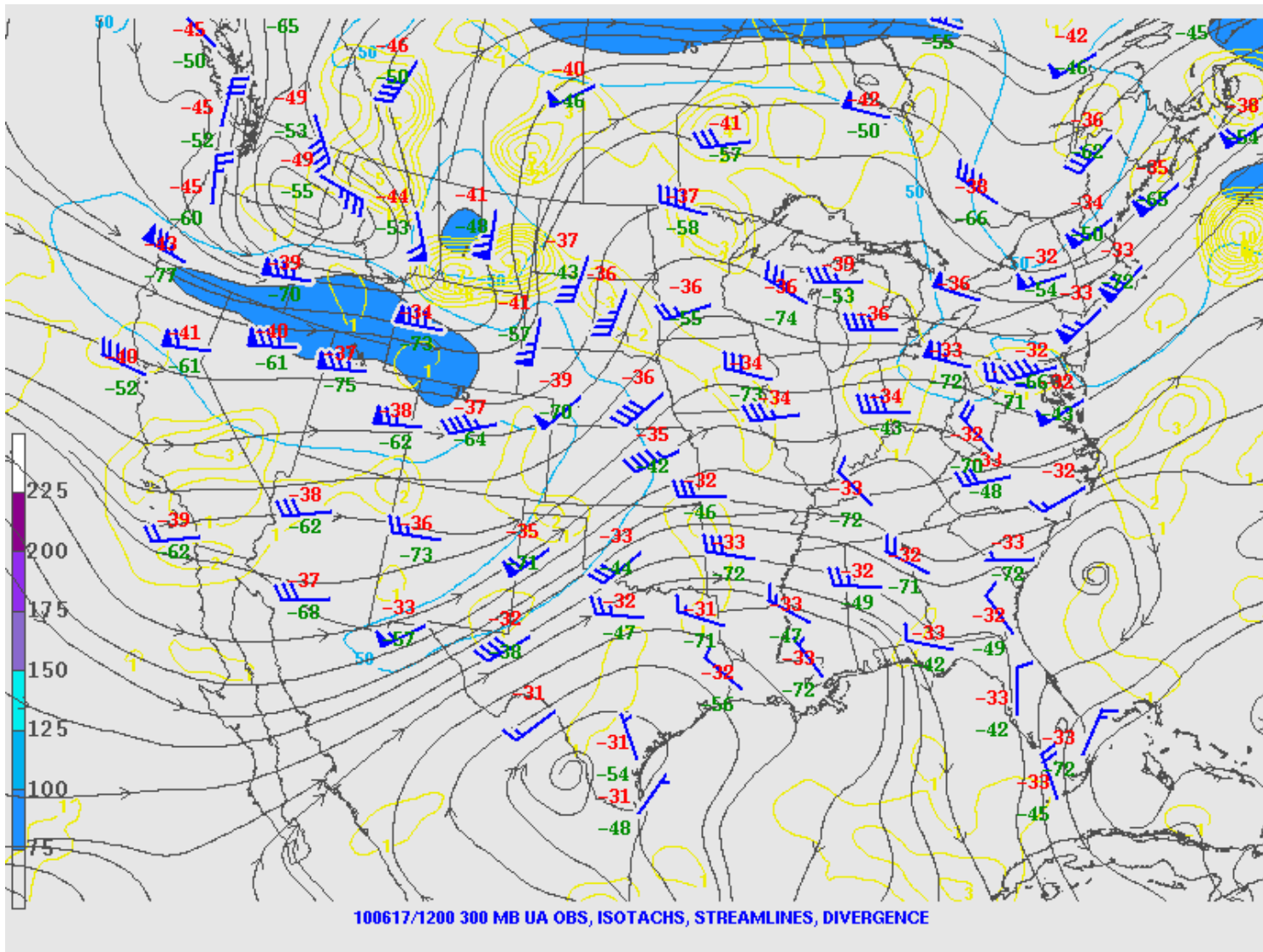


Fig 27: 1200 UTC 17 June 2010 300 hPa observations, streamlines, isotachs (shaded, kts), and divergence (contoured, s^{-1}).

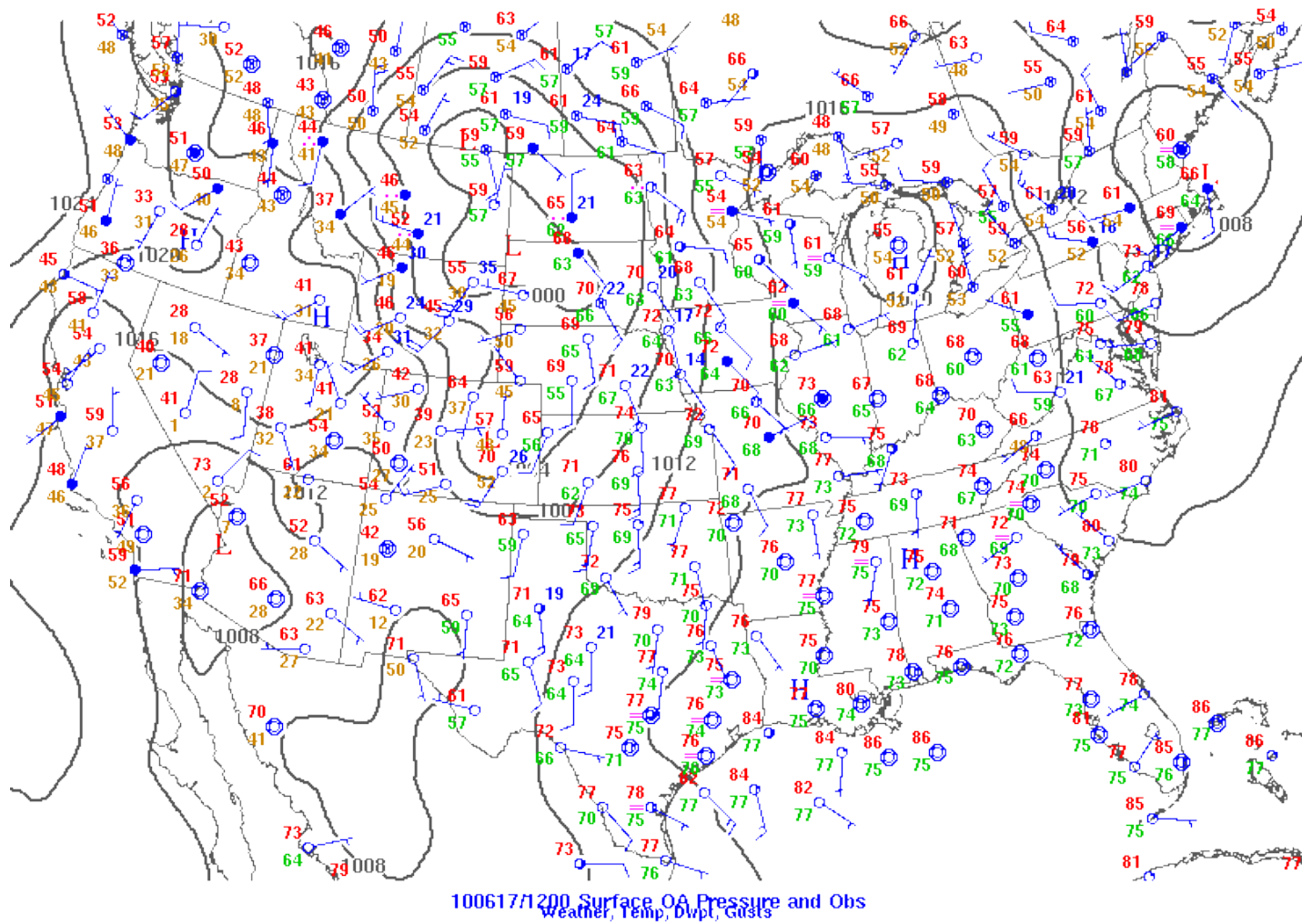


Fig 28: 1200 UTC 17 June 2010 surface observations and pressure analysis.

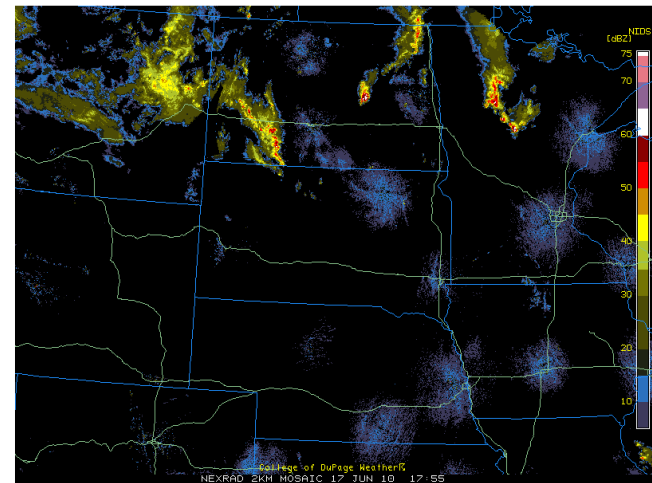
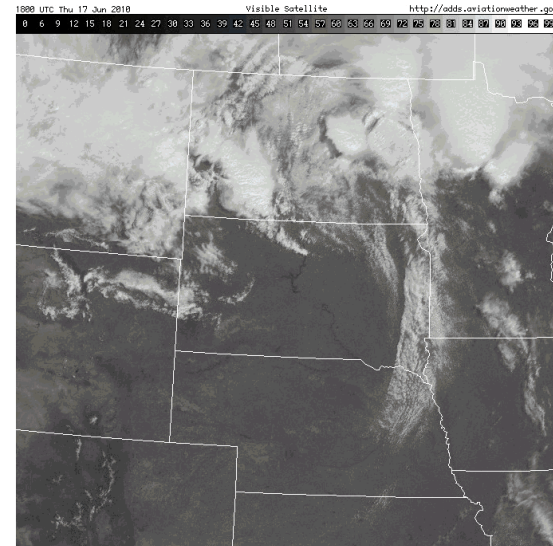
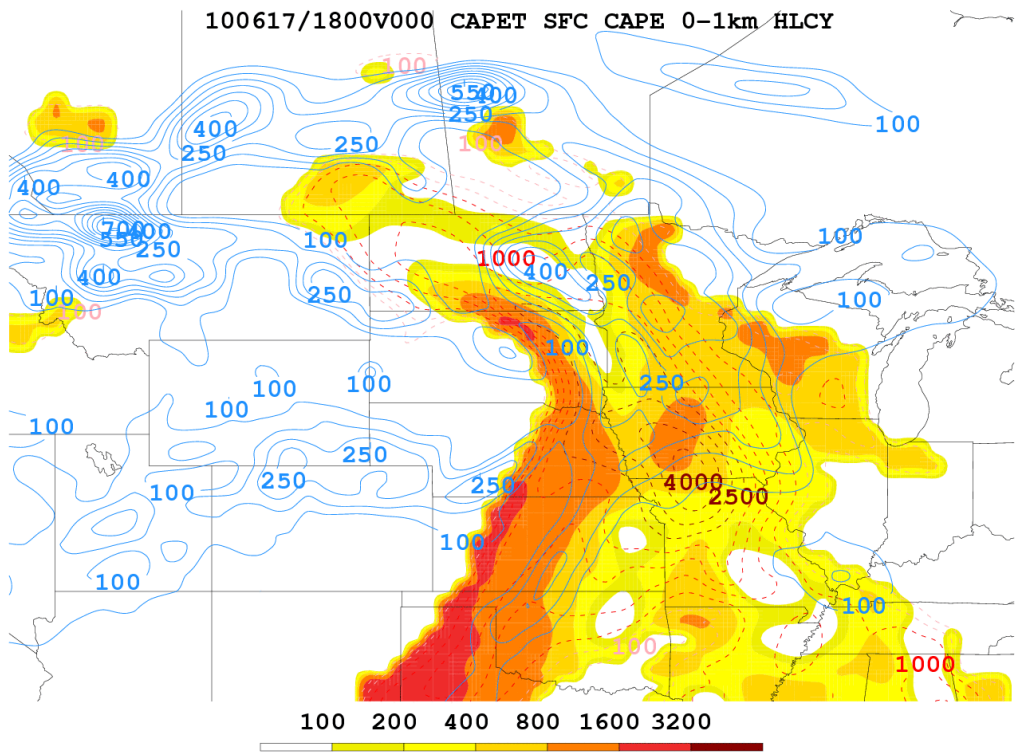


Fig 29. 1800 UTC 17 June 2010 CAPE Tendency Analysis with CAPE tendency (shaded), SBCAPE (hatched), and 0-1 km helicity (contoured). Upper Right: 1825 UTC satellite imagery. Lower Right: 1800 UTC radar composite.

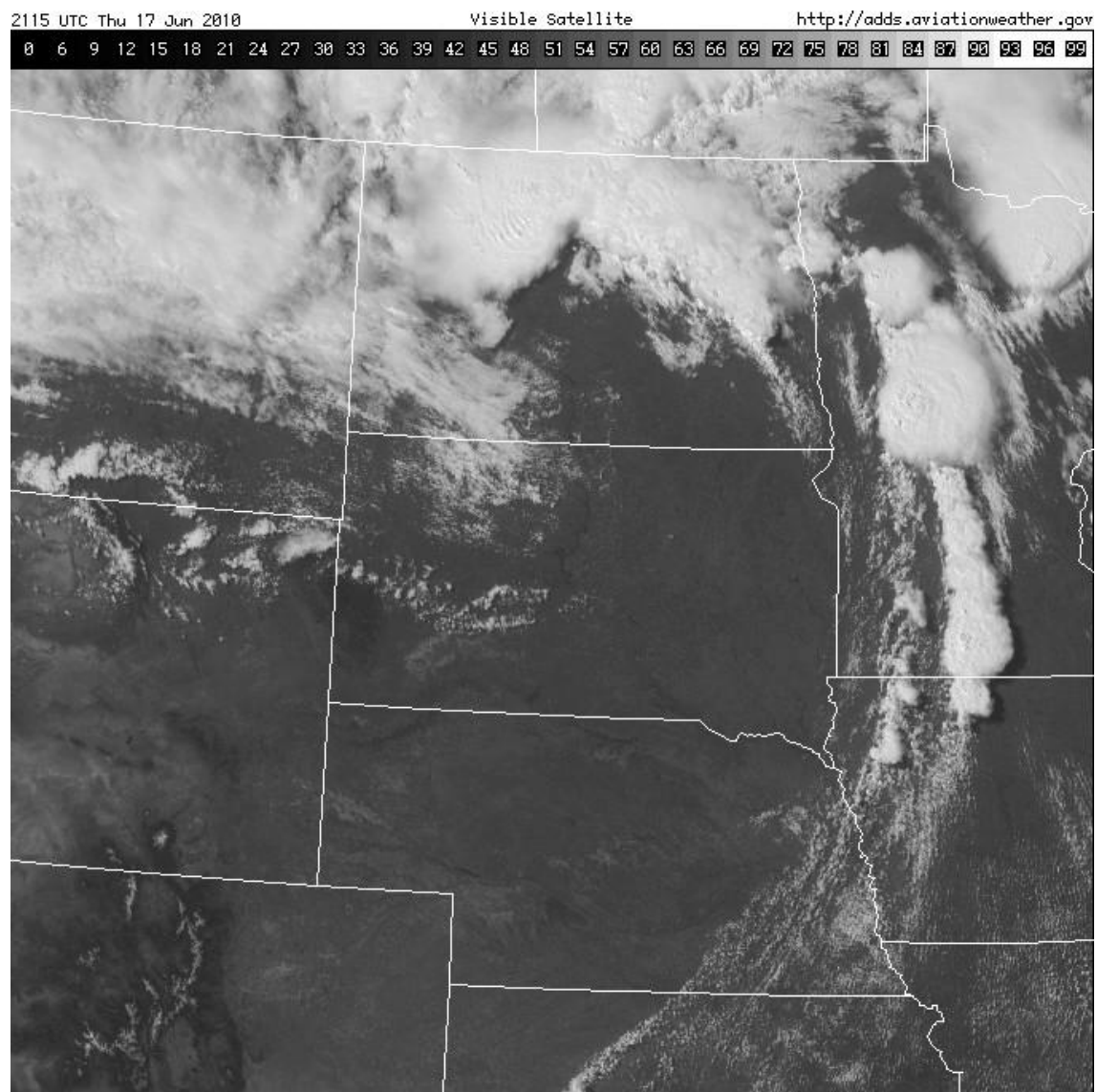


Fig 30. 2115 UTC 17 June 2010 satellite imagery indicating developing convection in Minnesota.

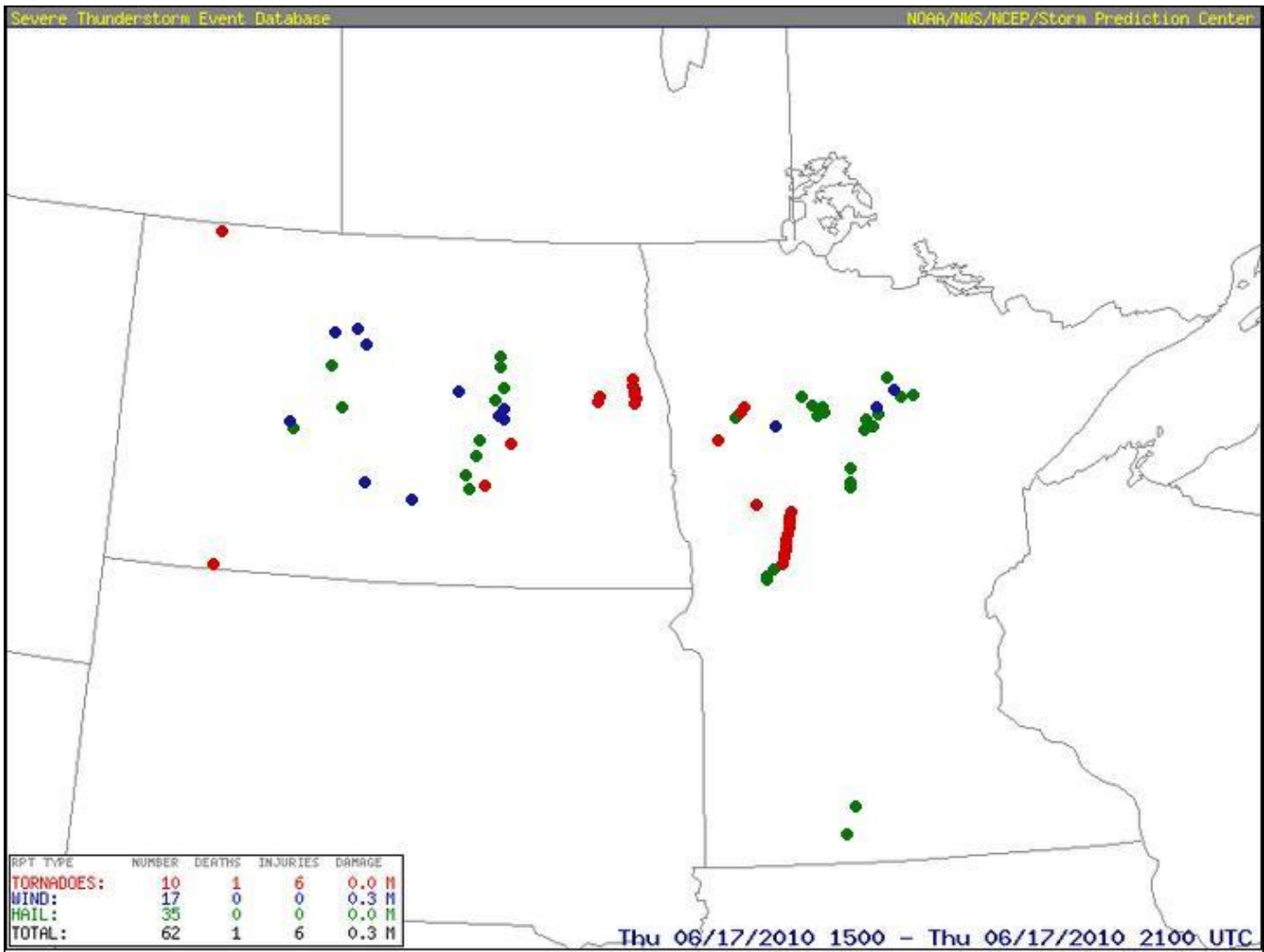


Fig 31: SPC storm reports from 1500 UTC to 2100 UTC 17 June 2010.

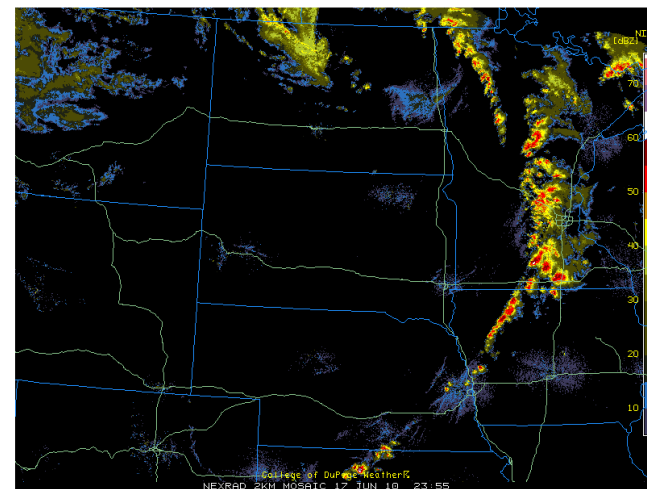
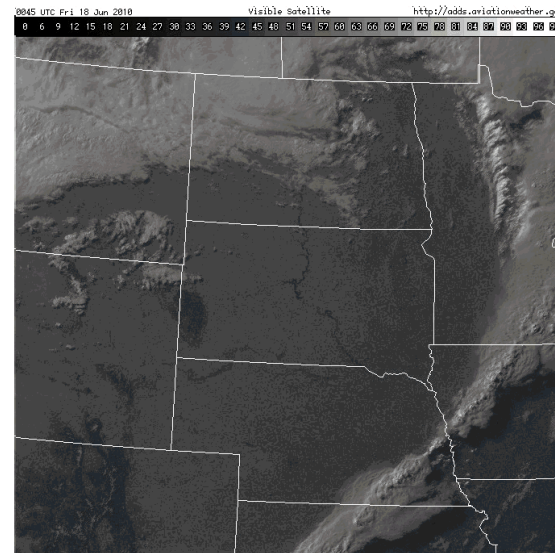
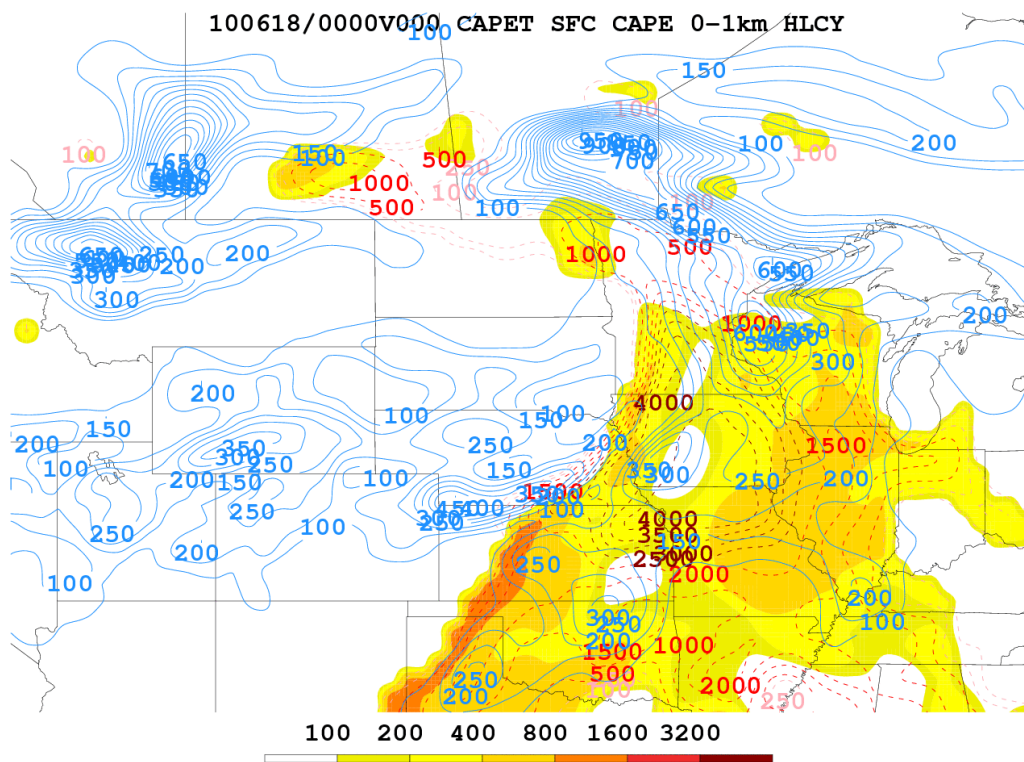


Fig 32. 0000 UTC 18 June 2010 CAPE Tendency Analysis with CAPE tendency (shaded), SBCAPE (hatched), and 0-1 km helicity (contoured). Upper Right: 0045 UTC satellite imagery. Lower Right: 0000 UTC radar composite.

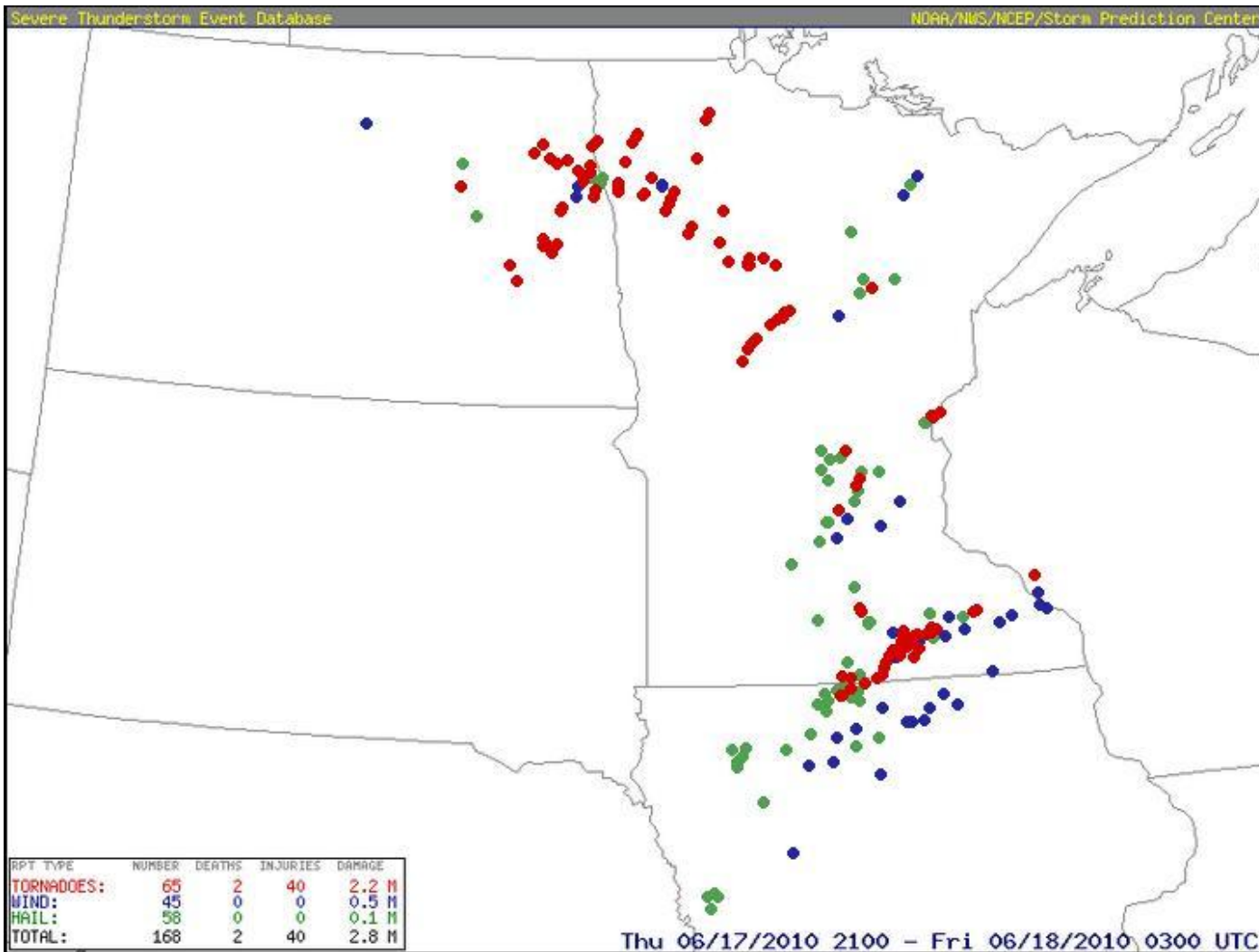


Fig 33. SPC storm reports from 2100 UTC 17 June 2010 to 0300 UTC 18 June 2010.

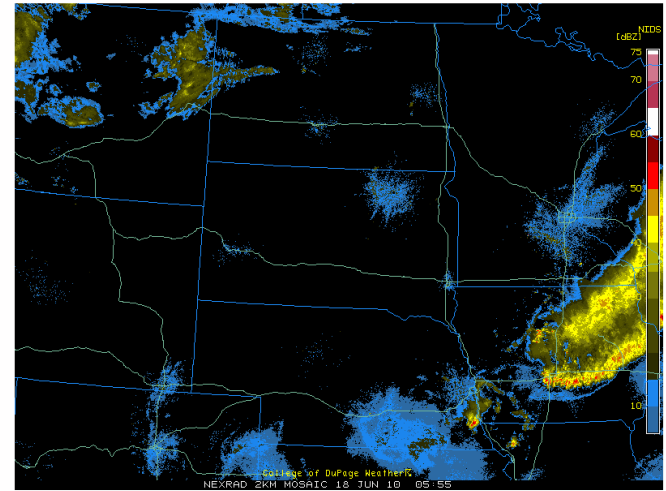
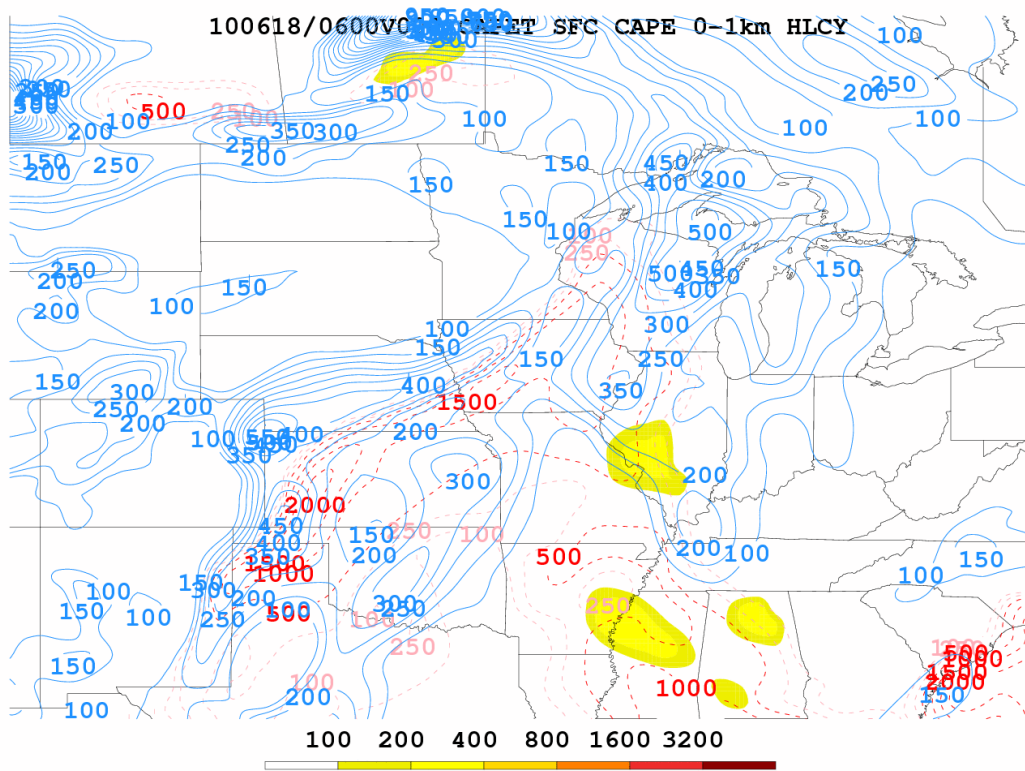


Fig 34. 0600 UTC 18 June 2010 CAPE Tendency Analysis with CAPE tendency (shaded), SBCAPE (hatched), and 0-1 km helicity (contoured). Right Side: 0600 UTC radar composite.